McCaig, A.M., Lang, S.Q., Blum, P., and the Expedition 399 Scientists
Proceedings of the International Ocean Discovery Program Volume 399
publications.iodp.org

Expedition 399 summary[1]

A.M. McCaig, S.Q. Lang, P. Blum, N. Abe, W. Brazelton, R. Coltat, J.R. Deans, K.L. Dickerson, M. Godard, B.E. John, F. Klein, R. Kuehn, K.-Y. Lin, C.J. Lissenberg, H. Liu, E.L. Lopes, T. Nozaka, A.J. Parsons, V. Pathak, M.K. Reagan, J.A. Robare, I.P. Savov, E. Schwarzenbach, O.J. Sissmann, G. Southam, F. Wang, and C.G. Wheat[2]

[1] McCaig, A.M, Lang, S.Q., Blum, P., Abe, N., Brazelton, W., Coltat, R., Deans, J.R., Dickerson, K.L., Godard, M., John, B.E., Klein, F., Kuehn, R., Lin, K.-Y., Lissenberg, C.J., Liu, H., Lopes, E.L., Nozaka, T., Parsons, A.J., Pathak, V., Reagan, M.K., Robare, J.A., Savov, I.P., Schwarzenbach, E., Sissmann, O.J., Southam, G., Wang, F., and Wheat, C.G., 2025. Expedition 399 summary. In McCaig, A.M., Lang, S.Q., Blum, P., and the Expedition 399 Scientists, Building Blocks of Life, Atlantis Massif. Proceedings of the International Ocean Discovery Program, 399: College Station, TX (International Ocean Discovery Program). https://doi.org/10.14379/iodp.proc.399.101.2025
[2] **Expedition 399 Scientists' affiliations.**

Contents

Keywords
International Ocean Discovery Program; IODP; *JOIDES Resolution*; Expedition 399; Building Blocks of Life, Atlantis Massif; Biosphere Frontiers; Earth Connections; Earth in Motion; Site U1309; Site U1601; serpentinization; Lost City hydrothermal field; ultramafic; peridotite; mantle; detachment fault; abiotic organic synthesis; geomicrobiology; deep biosphere; carbon budget; wireline logging

Core descriptions

Supplementary material

References (RIS)

MS 399-101
Published 3 May 2025

Funded by NSF OCE1326927, ECORD, and JAMSTEC

Abstract

International Ocean Discovery Program (IODP) Expedition 399 collected new cores from the Atlantis Massif (30°N; Mid-Atlantic Ridge), an oceanic core complex that hosts the Lost City hydrothermal field (LCHF). Studies of the Atlantis Massif and the LCHF have transformed our understanding of tectonic, magmatic, hydrothermal, and microbial processes at slow-spreading ridges. The Atlantis Massif was the site of four previous expeditions (Integrated Ocean Drilling Program Expeditions 304, 305, and 340T and IODP Expedition 357) and numerous dredging and submersible expeditions. The deepest IODP hole in young (<2 My) oceanic lithosphere, Hole U1309D, was drilled ~5 km north of the LCHF and reached 1415 meters below seafloor (mbsf) through a series of primitive gabbroic rocks. A series of 17 shallow (<16.4 mbsf) holes were also drilled at 9 sites across the south wall of the massif during Expedition 357, recovering heterogeneous rock types including hydrothermally altered peridotites, gabbroic, and basaltic rocks. The hydrologic regime differs between the two locations, with a low-permeability conductive regime in Hole U1309D and a high- (and possibly deep-reaching) permeability regime along the southern wall.

Expedition 399 targeted Hole U1309D and the southern wall area to collect new data on ancient processes during deformation and alteration of detachment fault rocks. The recovered rocks and fluids are providing new insights into past and ongoing water-rock interactions, processes of mantle partial melting and gabbro emplacement, deformation over a range of temperatures, abiotic organic synthesis reactions, and the extent and diversity of life in the subseafloor in an actively serpentinizing system. We sampled fluids and measured temperature in Hole U1309D before deepening it to 1498 mbsf. The thermal structure was very similar to that measured during Expedition 340T, and lithologies were comparable to those found previously in Hole U1309D. A significant zone of cataclasis and alteration was found at 1451–1474 mbsf. A new Hole U1601C (proposed Site AMDH-02A) was drilled on the southern ridge close to Expedition 357 Hole M0069A, where both deformed and undeformed serpentinites had previously been recovered. Rapid drilling rates achieved a total depth of 1267.8 mbsf through predominantly ultramafic (68%) and gabbroic (32%) rocks, far surpassing the previous drilling record in a peridotite-dominated system of 201 m. Recovery was excellent overall (71%) but particularly high in peridotite-dominated sections where recovery regularly exceeded 90%. The recovery of sizable sections of largely intact material will provide robust constraints on the architecture and composition of the oceanic mantle lithosphere. The deepest portions of the newly drilled borehole may be beyond the known limits of life, providing the means to assess the role of biological activity across the transition from a biotic to an abiotic regime.

Borehole fluids from both holes were collected using both the Kuster Flow-Through Sampler and the new Multi-Temperature Fluid Sampler. Wireline logging in Hole U1601C provided information on downhole density and resistivity, imaged structural features, and documented fracture orientations. A reentry system was installed in Hole U1601C, and both it and Hole U1309D were left open for future deep drilling, fluid sampling, and potential borehole observatories.

Plain language summary

The Earth's mantle is a thick (1802 miles; 2900 km) layer of dense rock that makes up most of the planet's mass. It has long been a goal to drill through the Earth's crust and into the upper mantle, but so far this has not been achieved, even in the oceans where the crust is relatively thin (6 km). In some places, mantle and lower crustal rocks have been brought to the seafloor by faulting associated with plate tectonics. One such place is the Atlantis Massif, an underwater mountain in the middle of the Atlantic Ocean. Mantle rocks are rich in the mineral olivine, and when they are altered by seawater they produce the mineral serpentine. Hydrogen is produced as a by-product of the reaction and can further fuel the generation of compounds such as methane, short-chain hydrocarbons, and organic acids in the absence of life. Hence, we can call these compounds "the building blocks of life" because when life began on Earth in the distant past, they may have been the precursors to more complex compounds, such as DNA, necessary for life to exist. At the present day, this suite of compounds may be feeding ancient forms of microbial life far below the seafloor.

The goals of Expedition 399 were to recover rocks and fluids to provide new insights into how underwater mountains such as the Atlantis Massif form, to document the abiological reactions between water and rocks that may represent ancient systems that preceded life on Earth, and to assess the extent of life in the subseafloor. We deepened preexisting Integrated Ocean Drilling Program Hole U1309D by 83 m to reach a new depth of 1498 meters below seafloor and sampled fluids to understand the geochemical regime. The recovered rocks were gabbroic, typical of the lower crust, and temperatures near the bottom of the borehole were ~140°C, similar to previous measurements. Drilling revealed a 23 m zone of fracturing and alteration.

A new Hole U1601C was also drilled on the southern wall of the massif and achieved a total depth of 1267.8 meters below seafloor with excellent overall recovery of 71%. It primarily consists of a long section of mantle rocks with intrusions of gabbro that cooled from injections of magma from depth. Previous drilling into this type of rock has not been nearly as successful and has previously only reached a maximum depth of 201 m. The recovery of sizable sections of largely intact mantle rocks will provide robust constraints on the structure and composition of the oceanic mantle lithosphere and the reactions that produce hydrogen. Downhole logging measurements were carried out to provide a continuous record of temperature, density, porosity, seismic velocity, and distributions of fractures. Water samples were collected from several depths within the borehole to determine the chemical and biological characteristics of fluids. Both Holes U1601C and U1309D were left open for future fluid sampling and potential borehole observatories.

1. Introduction

The Atlantis Massif oceanic core complex (OCC) (30°N; Mid-Atlantic Ridge; Figure **F1**) has been investigated during four drilling expeditions (Integrated Ocean Drilling Program Expeditions 304, 305, and 340T and International Ocean Discovery Program [IODP] Expedition 357) and numerous other cruises (Cann et al., 1997; Blackman et al., 1998; Kelley et al., 2001, 2005; Blackman et al., 2002, 2013; Karson et al., 2006; Canales et al., 2004, 2008; Lang et al., 2021). The southern wall of the massif hosts the Lost City hydrothermal field (LCHF), which has vented alkaline fluids rich in H_2 and CH_4 at temperatures of 40°–116°C for >100,000 y (Früh-Green et al., 2003; Ludwig et al., 2011; Kelley et al., 2005; Proskurowski et al., 2008; Seyfried et al., 2015). The LCHF is a model site for studying the serpentinization processes that lead to the creation of alkaline hydrothermal fluids rich in H_2 and CH_4, which are also proposed to occur on other planetary bodies. The Atlantis Massif has also been targeted by multiple expeditions to study the crustal accretion and OCC formation at slow-spreading ridges. Although previous expeditions to this site have sought to characterize these and other processes, drilling has yet to recover ultramafic rocks that are characteristic of the conditions thought to occur deep beneath the LCHF. To address these gaps in knowledge, the goal of the current expedition was to collect deeper cores from the Atlantis Massif from both Integrated Ocean Drilling Program Hole U1309D (proposed Site AMDH-01A) as well as from the southern wall in the footprint of shallower drilling carried out during Expedition 357 (Figures **F1**, **F2**, **F3**).

Hole U1309D in the central dome of the Atlantis Massif is located in the footwall to a large slip oceanic detachment fault system (Blackman et al., 2004; Blackman, Ildefonse, John, Ohara, Miller, MacLeod, and the Expedition 304/305 Scientists, 2006; Grimes et al., 2008) and penetrated largely gabbroic rocks to 1415 meters below seafloor (mbsf) (Figures **F1**, **F2**, **F3**, **F4**). This site contrasts with the southern wall of the massif near the LCHF, which predominantly consists of serpentinized peridotite with ~20% gabbroic rocks (Figures **F1**, **F3**, **F5**), and was extensively sampled by shallow coring during Expedition 357 (Früh-Green et al., 2018; Schroeder and John, 2004; Karson et al., 2006). At the top of the massif is an oceanic detachment fault zone largely formed in serpentinites and minor gabbros above the southern wall and gabbros in Hole U1309D. Syntectonic diabase dikes intrude the fault rocks and are in turn deformed at both localities. Fault rocks include talc-tremolite-chlorite schists overprinting serpentinite, with fault breccias and cataclasites locally overprinting higher temperature fault rocks including amphibolites (Blackman et al., 2011; McCaig et al., 2010; McCaig and Harris, 2012).

During Expedition 399, we revisited Hole U1309D in the central dome of the massif and also drilled two new holes at Site U1601 (proposed Site AMDH-02A), within the footprint of Expedition 357 on the southern wall (Figures **F1**, **F2**, **F3**; Table **T1**).

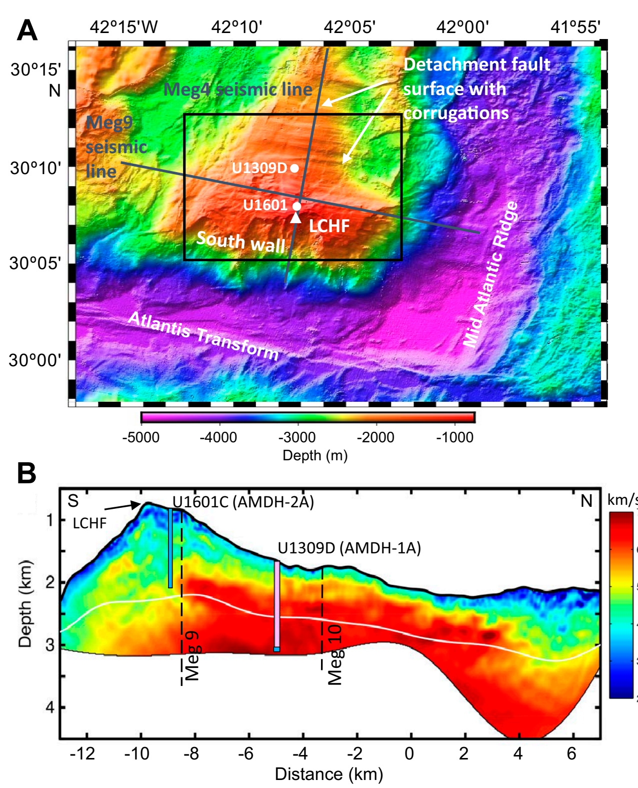

Figure F1. A. Atlantis Massif showing main structural features, location of LCHF, Hole U1309D, and Site U1601 (core recovered in Holes U1601A and U1601C). Bathymetry was collected during Expedition 357 (Früh-Green et al., 2018; Escartín et al., 2022). Adapted from Cotterill and Früh-Green (2021). Box = area of Figure F2. B. Full waveform inversion of Seismic Line Meg 4 and locations of Holes U1309D and U1601C, with proposed site numbers. Blue = new core recovered during Expedition 399, pink = core from Expedition 304/305. Modified after Harding et al. (2016).

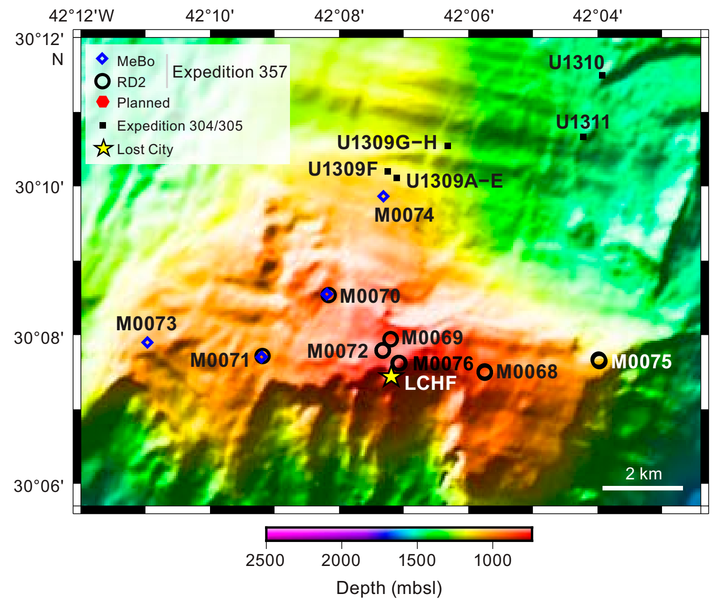

Figure F2. Location of previous drilling during Expeditions 304/305 and 357 (modified after Früh-Green et al., 2016). MeBo = Meeresboden-Bohrgerät 200 drill, RD2 = RockDrill2 drill. Expedition 399 sites are at Site U1309 (Hole U1309D; labeled U1309A–E) and between Sites M0069 and M0072 (Site U1601).

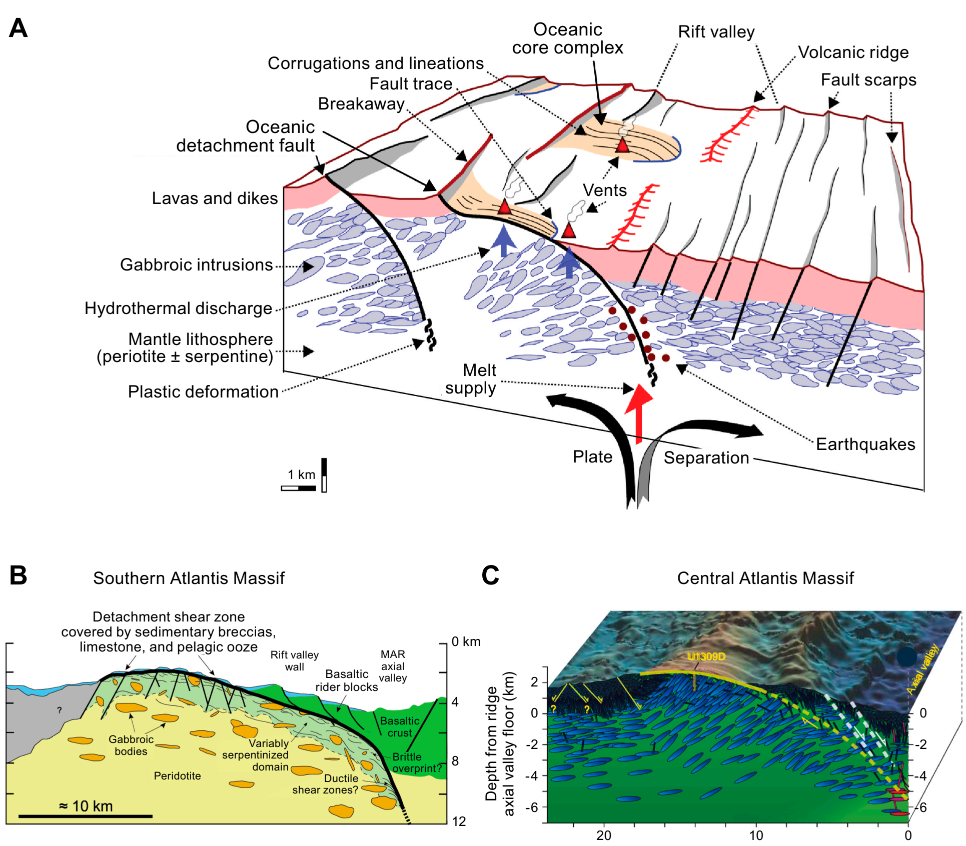

Figure F3. Conceptual sketches of tectonomagmatic evolution of heterogeneous lithosphere and denudation of mantle rocks as detachment faulting progresses (Früh-Green et al., 2016). A. Generic "detachment mode" seafloor (Escartín and Canales, 2011). B. Southern wall of Atlantis Massif is dominated by variably altered peridotites with gabbroic lenses (Boschi et al., 2006). 100 m thick detachment fault zone containing talc-tremolite-chlorite metasomatic schists is at the summit (Karson et al., 2006). MAR = Mid-Atlantic Ridge. C. In contrast, major gabbroic intrusions dominate the central dome (Grimes et al., 2008).

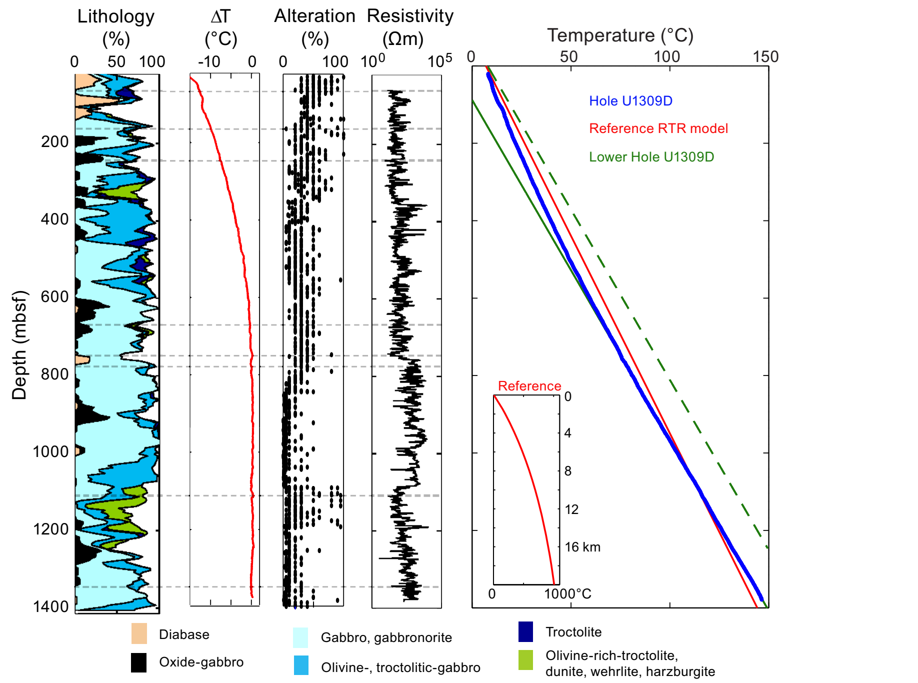

Figure F4. Lithology, temperature, and resistivity logging results, Expeditions 304/305 and 340T and Hole U1309D (after Blackman et al., 2014). ΔT = difference between observed temperature and extrapolation of conductive gradient at depth to surface. Minor excursions in temperature are interpreted to be zones of fluid flow at 746 mbsf, where temperature gradient changes from convective to conductive, and 1107 mbsf, near a zone of olivine-rich troctolite.

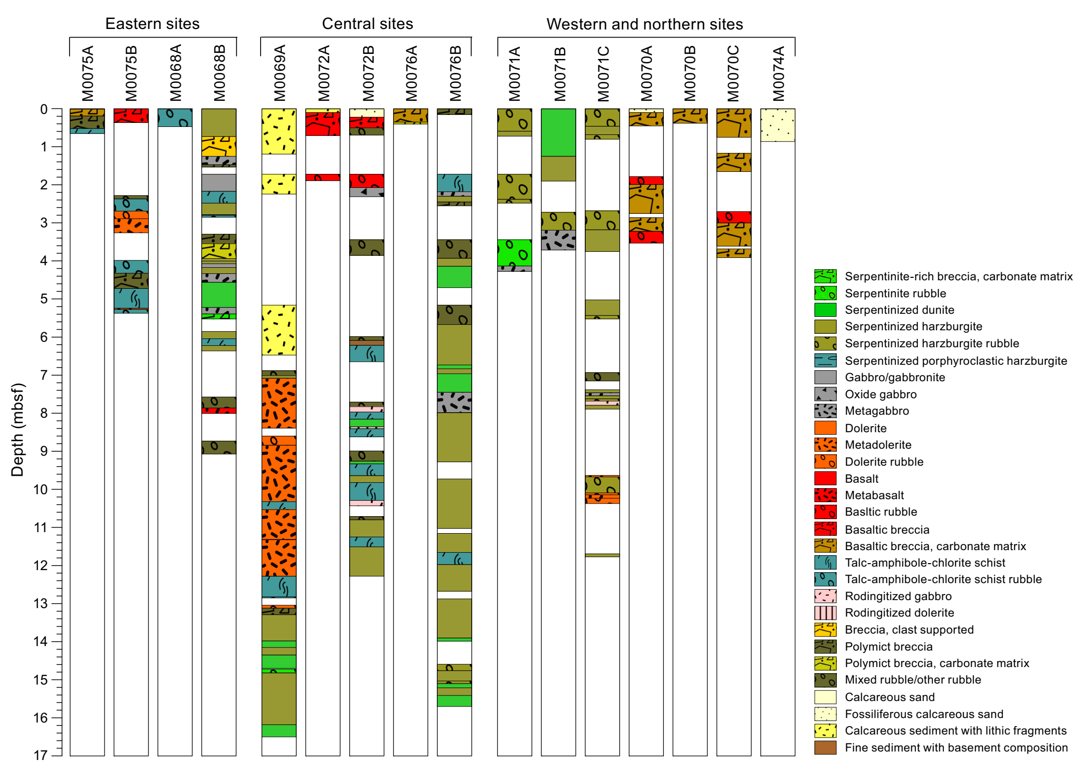

Figure F5. Lithologic summaries from Expedition 357 holes along southern wall of Atlantis Massive (from Früh-Green et al., 2016). Site U1601 is close to Hole M0069A, where metadolerite (metadiabase) intrudes into talc-tremolite-chlorite schists, both of which are brecciated and underlain by subhorizontal brittle fault zone at ~13 mbsf. Below this fault are little-deformed serpentinized harzburgite and dunite. Beneath soft-sediment layer, hole recovery was excellent.

Table T1. Hole summary, Expedition 399. DSF = drilling depth below seafloor. RCB = rotary core barrel. MTFS = Multi-Temperature Fluid Sampler, ETBS = Elevated Temperature Borehole Sensor, KFTS = Kuster Flow-Through Sampler. **Download table in CSV format.**

Hole	Latitude	Longitude	Water depth (m)	Total penetration DSF (m)	Cored interval (m)	Recovered length (m)	Recovery (%)	Drilled interval (m)	Drilled interval (*N*)	Total cores (*N*)	RCB cores (*N*)	Other cores (*N*)
399-												
U1309D	30°10.1195′N	42°7.1131′W	1644.9	82.5	82.5	48.93	59		0	17	17	1
U1601A	30°7.9260′N	42°7.2255′W	850.0	60.6	60.6	14.52	24		0	12	12	0
U1601B	30°7.9339′N	42°7.2171′W	850.0	26.0			0	26.0	1	0	0	0
U1601C	30°7.9417′N	42°7.2072′W	850.0	1267.8	1244.8	886.03	71	23.0	1	257	257	1
			Expedition 399 totals:	1436.9	1387.9	949.48		49.0	2	286	286	2

Hole	Temperature and fluid sampling with MTFS-ETBS	Temperature and fluid sampling with dual KFTS-ETBS	Geophysical wireline logging	Date started (2023)	Start time UTC (h)	Date finished (2023)	End time UTC (h)	Time on hole (d)
399-								
U1309D	1 coreline run	5 coreline runs		25 Apr	0715	4 Jun	0430	8.08
U1601A				19 Apr	0545	22 Apr	1730	3.49
U1601B				22 Apr	1730	25 Apr	0715	2.54
U1601C		4 coreline runs	5 tool strings	1 May	2245	2 Jun	1800	31.80
						Expedition 399 totals:		45.91

2. Background

2.1. Previous holes in basement rocks

Several previous Deep Sea Drilling Project (DSDP)/Ocean Drilling Program (ODP)/Integrated Ocean Drilling Program/IODP expeditions have succeeded in drilling holes deeper than 100 m into the igneous basement, and they highlight the scientific value of both the recovered material and the borehole itself (Figure **F6**). The deepest is DSDP Hole 504B, which succeeded in drilling into the sheeted dike complex in the Nazca plate. Hole 504B has been visited repeatedly for water sampling and hydrogeology experiments (Magenheim et al., 1995; Becker et al., 2004; Teagle, Alt, Umino, Miyashita, Banerjee, Wilson, and the Expedition 309/312 Scientists, 2006).

Two deep boreholes, ODP Hole 735B and IODP Hole U1473A, were drilled into gabbro on the Atlantis Bank, SW Indian Ridge (Table **T2**; Natland and Dick, 2002; Dick et al., 2017). The second deepest is Hole U1309D in the Atlantis Massif, which is by far the deepest basement hole in young (<2 Ma) lithosphere (Blackman et al., 2011). Most successful drilling has occurred in OCCs or slow-spread crust because the gabbroic layer in fast-spread crust has proved very hard to reach. The exceptions are ODP Leg 147 Hole 894B (Gillis, Mével, Allan, et al., 1993) and Integrated Ocean Drilling Program Hole U1415P, which recovered layered gabbros near the base of the faulted rift wall of the Cocos Plate at Hess Deep (Gillis et al., 2014).

Very few expeditions have recovered significant lengths of mantle rocks. Two holes from Leg 147 to Hess Deep Rift (Holes 895D and 895E) penetrated 93.7 and 87.6 m, respectively (Gillis, Mével, Allan, et al., 1993). Six holes were started at this site, coring 272.9 m but recovering only 64.6 m. Up to 150 m of ultramafic basement rock was also drilled at the passive continental Iberian Margin during ODP Legs 149 and 173 (Sawyer et al., 1994; Whitmarsh et al., 1998). All the other boreholes drilled into mantle rocks are located on the slow-spreading Mid-Atlantic Ridge, including ODP Leg 153 Holes 920B and 920D (23°N; Mid-Atlantic Ridge; Cannat, Karson, Miller, et al., 1995) and ODP Leg 209 Holes 1271B, 1272A, 1268A, and 1274A (12°–16°N; Mid-Atlantic Ridge; Kelemen, Kikawa, Miller, et al., 2004). At 200.9 m, Hole 920D is the deepest hole drilled in mantle rocks prior to this expedition. Peridotite can only be exposed on the seafloor by faulting, and drilling fault rocks has contributed to the poor recovery and penetration of previous holes.

Previous holes in serpentinized peridotite have often hosted significant thicknesses of gabbroic rock and have led to important insights into the nature of slow-spread lithosphere (Cannat, 1996) and processes such as melt-rock reaction, deformation, and serpentinization (Coogan et al., 2000a, 2000b; Karson et al., 1997). However, poor recovery has hampered systematic study of relationships, and drilling a deep hole into serpentinized and fresh peridotite was one of the main aims of Expeditions 304 and 305 in the Atlantic Massif (Blackman et al., 2004). This aim was frustrated when 1415 m of gabbroic rocks was recovered instead.

2.2. Geologic setting

The Atlantis Massif is an inside corner high on the right-stepping, sinistral, Atlantis I transform fault at 30°N on the Mid-Atlantic Ridge (Figure **F1**). The massif formed within the last 1.2–2 My (Grimes et al., 2008; Escartín et al., 2022). It was the first corrugated massif identified as an OCC (Cann et al., 1997), and it is capped by a domal detachment fault with corrugations parallel to the spreading direction (Figure **F3**). To the east, the detachment surface disappears beneath a hanging

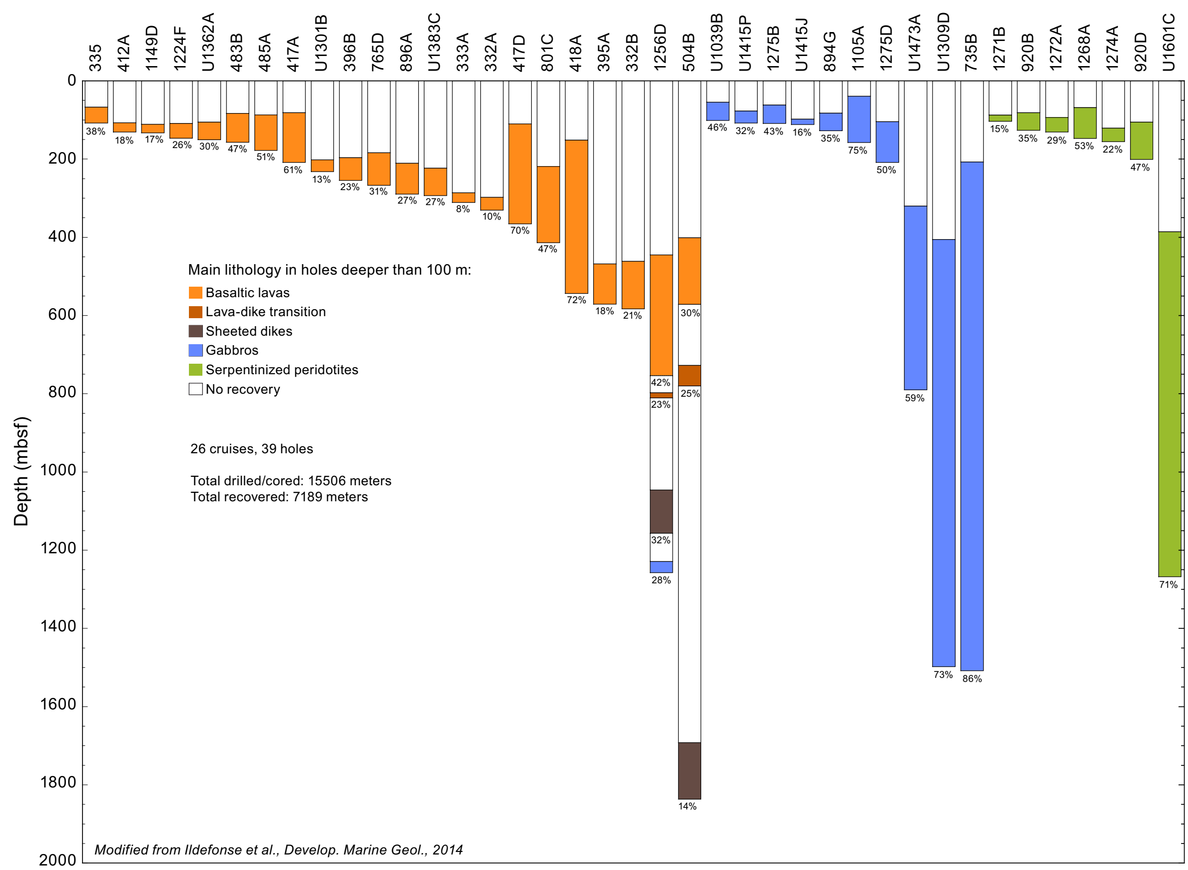

Figure F6. Summary of all DSDP/ODP/IODP holes with >100 m basement penetration (modified after Ildefonse et al., 2014), with Hole U1309D updated to reflect additional penetration during Expedition 399 and Hole U1601C added.

Table T2. Summary of holes drilled >750 m into oceanic lithosphere. **Download table in CSV format.**

Hole	Depth (mbsf)	Total bit runs (including logging)	Leg/Expedition	Site name	Latitude	Longitude
U1473A	790	24	IODP Expedition 360	Atlantis Bank, Southwest Indian Ridge	32°42.340′S	57°16.691′E
U1601C	1267	8	IODP Expedition 399	Atlantis Massif	30°7.942′N	42°7.207′W
U1309D	1498	12	Integrated Ocean Drilling Program Expeditions 304 and 305 and IODP Expedition 399	Atlantis Massif	30°10.120′N	42°7.113′W
735B	1508	14	ODP Legs 118 and 176	Atlantis Bank, Southwest Indian Ridge	32°43.395′S	57°15.959′E
1256D	1522	62	ODP Leg 206 and Integrated Ocean Drilling Program Expeditions 309, 312, and 335	Guatemala Basin	6°44.16′N	91°56.06′W
504B	2111	98	DSDP Legs 69, 70, 83, and 93 and ODP Legs 111, 137, 140, and 148	Costa Rica Rift	1°13.611′N	83°43.818′W

wall composed of fresh basaltic rocks and is truncated by steep east-facing median valley faults. Recent interpretations (Escartín et al., 2022) suggest that a relic of the detachment fault has been trapped in the bottom of the axial valley by a westward ridge jump. To the west, a breakaway is assumed to be present but has never been unequivocally located. The shallowest part of the massif is at the top of the south wall, with a depth <700 meters below sea level (mbsl), and the detachment fault slopes north toward the central massif, where Site U1309 is located. To the north, the detachment is inferred to disappear beneath faulted blocks of basalt.

Early work on the massif concentrated on dredging and submersible studies along the south wall and to a lesser extent the dome (Figure **F3B**), which is dominated by serpentinized peridotite with inclusions of gabbro (Cann et al., 1997; Blackman et al., 1998, 2002). This slope is a transform fault wall degraded by slope failure, and it may be the substrate supporting the LCHF (Kelley et al., 2001, 2005). Geophysical surveys include a refraction experiment (Detrick and Collins, 1998) and multichannel seismic (MCS) profiles (Canales et al., 2004). High velocities were inferred from the refraction data and interpreted to be fresh peridotite at shallow depths. However, Hole U1309D (drilled during Expeditions 304 and 305 in 2004 and 2005) showed that the central massif was floored predominantly by gabbro to at least 1415 mbsf (Figures **F3**, **F4**), requiring reevaluation of the internal structure of the Atlantis Massif and the geophysical interpretation (Blackman et al., 2011). Canales et al. (2008) reprocessed the MCS data in terms of *P*-wave tomography, showing high velocities in the central massif and lower velocities under the South Ridge, with a steep contact between a gabbroic domain and a serpentinite domain to the south. Further processing of the MCS data by Henig et al. (2012) improved the resolution of the imaging, and full waveform inversion (Figure **F1B**) by Harding et al. (2016) produced sharper and more detailed images, groundtruthed by the deep Hole U1309D (Figure **F4**). It remains very difficult to resolve variably serpentinized peridotite from variably altered gabbro beneath the South Ridge, but an irregular intrusive contact between gabbro and partially serpentinized peridotite seems likely.

Hole U1309D was revisited during Expedition 340T (Blackman et al., 2013, 2014), which carried out an extensive wireline logging program, including a vertical seismic profile (VSP) and a temperature profile. The temperature gradient was nearly linear below 750 mbsf, indicating a conductive thermal gradient in the lower part of the hole.

Paleomagnetic data from Hole U1309D frequently show multicomponent remanences, mainly in the upper part of the hole (Morris et al., 2009; John et al., 2009). Inclinations of the primary remanence are shallower than expected at 30°N, and integration of paleomagnetic data with Formation MicroScanner (FMS) logging has allowed the declination of primary remanence to be constrained, indicating at least 45° of anticlockwise rotation about a ridge-parallel axis (Morris et al., 2009; Pressling et al., 2012). The section sampled in Hole U1309D was therefore likely dipping at <45° west when it formed, and interpretation of all high-temperature events should be interpreted in terms of distance from an originally steep detachment fault at depth, rather than the seafloor (cf. McCaig and Harris, 2012)

Expedition 357 was a mission-specific platform expedition during which a series of 17 shallow holes were drilled (to a maximum of 16.4 mbsf) at 9 locations in the southern part of the massif using seabed drills (Figures **F1**, **F2**, **F5**) (Früh-Green et al., 2017, 2018). The majority of the sites were located along an 8.5 km east–west profile perpendicular to the plate spreading on the Mid-Atlantic Ridge, accessing lithosphere of distinct ages. Two sites were drilled on the eastern part, closest to the spreading center (Sites M0068 and M0075), three sites were drilled in the central section north of the LCHF (Sites M0069, M0072, and M0076), and two sites were drilled on the western end (Sites M0071 and M0073). Excellent sections were collected of heterogeneous rocks through fault and alteration zones from these drill sites. The cores from the central sites at the top of the massif and closest to Lost City were predominantly composed of pervasively serpentinized harzburgite. Mafic rocks were less prevalent in these central locations compared to Hole U1309D, suggesting a different mode of melt accumulation. Two additional locations were drilled closer to the central dome of the massif (Sites M0070 and M0074) to target the mafic, plutonic domain drilled at Site U1309 but with limited recovery of only surficial material.

2.3. Igneous petrology

Rocks recovered from Hole U1309D include a sequence of gabbro and olivine gabbro (Figures **F4**, **F7**) with intervals of troctolite and olivine-rich troctolite and several diabase intrusions in the uppermost 100 m of the hole (Blackman, Ildefonse, John, Ohara, Miller, MacLeod, and the Expedition 304/305 Scientists, 2006; Blackman et al., 2011). Back-correcting for rotation, the diabase intrusions in the detachment zone could represent a lateral dike–gabbro transition (McCaig and Harris, 2012). Olivine-rich troctolites are interpreted to be mantle rocks modified by melt-rock reaction (Drouin et al., 2009, 2010; Ferrando et al., 2018); less modified mantle rocks are confined to very short intervals (<1 m) at shallow depths. The petrology and geochemistry of these mantle peridotite–derived samples were studied by Tamura et al. (2008). The gabbro contains many internal contacts (Suhr et al., 2008; John et al., 2009) and local igneous layering. Plutonic rocks recovered from Hole U1309D are among the most primitive ever recovered from the ocean floor in Holes U1309B and U1309D (Godard et al., 2008) (Figure **F7**). Unlike other drilled plutonic sections (Pacific Ocean: DSDP Hole 147 and ODP Hole 1256D; Indian Ocean: ODP Holes 735B and 1105A and Hole U1473A), many of the Atlantis Massif plutonic rocks are in equilibrium with mid-ocean-ridge basalt (MORB), with some primitive enough to have formed directly from primary mantle melts. Furthermore, they record significant isotopic heterogeneity, attesting to the delivery of individual batches of mantle melt to the plutonic section (Lambart et al., 2019). Hence, the Atlantis Massif offers a unique opportunity to study the compositions of melts delivered to the crust from their mantle source and how they evolve to MORB. This is paramount; crustal evolution of melt is now recognized to be significantly more complicated than previously realized, involving not only fractional crystallization but also in situ crystallization and reactive porous flow (Lissenberg and MacLeod, 2017). Hence, interpreting MORB compositions and implications for the upper mantle is highly nonunique, unless melt evolution processes in the lower crust are quantified (Godard et al., 2009).

The sequence of rocks on the south wall of the Atlantis Massif beneath Lost City has been summarized by Karson et al. (2006) and consists largely of highly serpentinized peridotites with gabbroic intervals (Figure **F3**). Gabbros here and in Expedition 357 cores have an uncertain relationship to the main gabbro farther north. They may be intrusions of different age or level of exhumation, or they may be satellites of the larger body. Establishing the genetic relationship between these bodies is important.

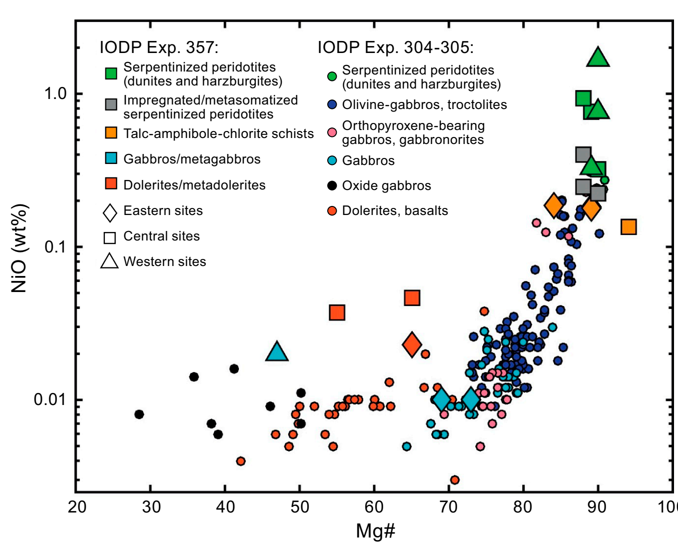

Figure F7. Summary of bulk rock igneous compositions, Hole U1309D (Expedition 304/305; Godard et al., 2009) and Expedition 357 core samples (Früh-Green et al., 2018). Note very primitive compositions of many of the gabbroic rocks compared to diabase (dolerite) dikes, which are similar to MORB at 30°N in Atlantic. Mg# = 100 × Mg/(Mg + Fe). Reprinted from Lithos (v. 323), Früh-Green et al., "Magmatism, serpentinization and life: insights through drilling the Atlantis Massif (IODP Expedition 357)," pages 137–155, Copyright (2018), with permission from Elsevier.

2.4. Structural and alteration history of the massif

The overall structure of the Atlantis Massif is domal with much of the top showing spreading-parallel corrugations identified as a low-angle detachment fault. To the east the detachment fault plunges beneath hanging wall basalts and locally dips toward the transform valley to the south (Escartín et al., 2022). Holes drilled at the top of the massif were expected to pass through the detachment fault zone, estimated by Karson et al. (2006) to be ~100 m thick (Figure **F3**).

The Hole U1309D section is remarkable for the paucity of high-temperature crystal-plastic fabrics compared to the only other deep holes into the footwall of OCCs, including the Atlantis Bank (Dick et al., 2017; Ildefonse et al., 2007; McCaig et al., 2010). However, significant breccia intervals occur in the uppermost 100 m of Holes U1309B and U1309D (Blackman et al., 2011). These both deform and are cut by syntectonic diabase intrusions common in the same interval (Figures **F4**, **F5**). Brecciation is inferred to have occurred over a wide range of temperatures up to >700°C (McCaig and Harris, 2012). Alteration is pervasive in the upper part of Hole U1309D, and isotopic data show the detachment fault zone to be highly altered by seawater-derived fluids at temperatures similar to black smoker fluids (McCaig et al., 2010). Greater intensities of crystal-plastic deformation were found in gabbroic lenses in peridotite on the south wall of the massif (Schroeder and John, 2004) and in the shallow cores from Expedition 357 (Früh-Green et al., 2018).

Intense alteration in the shallow Expedition 357 cores (Früh-Green et al., 2018; Rouméjon et al., 2018a) is generally consistent with previous work on the south wall (Boschi et al., 2006). Early serpentine replacing olivine is locally overprinted by talc-tremolite-chlorite assemblages frequently associated with mafic intrusions and/or shearing, and late-stage intense oxidation of the serpentinite mesh texture (Früh-Green et al., 2018). Carbonate veining is surprisingly rare and almost exclusively observed at the drill sites closest to the LCHF (Ternieten et al., 2021). Extensive water-rock interaction at variable temperatures is further reflected in heterogeneous sulfur isotope compositions (Liebmann et al., 2018). These document a complex evolution of the hydrothermal system with episodes of low-temperature serpentinization and incorporation of seawater sulfate facilitating microbial activity and episodes of high-temperature water-rock interaction controlled by the intrusion of microgabbroic veins, accompanied by considerable mass transfer.

Alteration in Hole U1309D records progressive fluid influx during cooling from magmatic to ambient temperatures. It is pervasive above 300 mbsf, with olivine-plagioclase reactions forming amphibole and chlorite in characteristic corona textures, reflecting temperatures above 500°C (Nozaka and Fryer, 2011). Deeper, the corona texture is restricted to the vicinity of fault zones and lithologic contacts, but partial serpentinization of olivine is common in many intervals and frequently accompanied by prehnite and hydrogarnet replacing plagioclase (Frost et al., 2008). Serpentinization reactions are complex, including early brucite-antigorite veins followed by more pervasive lizardite-magnetite (Beard et al., 2009). Olivine alteration in gabbros at low temperatures often produces saponite (Nozaka et al., 2008). Saponite in harzburgite has been observed to host nitrogenous compounds, including the amino acid tryptophan, which may be synthesized abiotically (Ménez et al., 2018). Alteration of Sr isotope ratios by seawater-derived fluids is common in the upper part of the hole but decreases below 350 mbsf and is mainly present in serpentine-rich intervals where the primary Sr content is low and the seawater signal may be carried by carbonates (McCaig et al., 2010). Alteration of oxygen isotope ratios away from primary igneous values is more persistent but also reduces downhole, affecting only visibly altered rocks. $\delta^{18}O$ is almost always <5.7‰ (the average composition of unaltered mantle and oceanic crust), indicating that the dominant reactions were at temperatures >200°–250°C (McCaig et al., 2010), where the fractionation between rock and water is <5.7‰. This is further supported by in situ $\delta^{18}O$ signatures in serpentine mesh textures from Expedition 357 cores that indicate serpentinization temperatures of 260°–360°C at increasing time-integrated water/rock ratios (Rouméjon et al., 2018b).

Reaction porosity and permeability produced by dissolution of minerals at the grain scale or greater is common in the upper part of Holes U1309B and U1309D and has been found in chloritized gabbros in Expedition 357 cores (McCaig et al., 2022). Rapid dissolution of primary minerals can occur if far from equilibrium hot fluid is in excess, as is likely in the upflow zone of a black smoker system (Cann et al., 2015).

Initial cooling of the massif was rapid based on paleomagnetic (Morris et al., 2009), geochronological, and thermochronological data (Grimes et al., 2008; Schoolmeesters et al., 2012) and diffusion timescales (Ferrando et al., 2020). This may have been linked to circulation of black smoker fluids in the detachment fault zone (McCaig et al., 2010; McCaig and Harris, 2012) in an early phase of circulation compared to the current phase of lower temperature venting at the LCHF.

2.5. Present-day thermal structure and hydrothermal circulation

Expedition 340T (Blackman et al., 2014) found that the temperature profile in Hole U1309D was conductive below 750 mbsf, with a gentle curvature suggesting slow downflow of fluid above that depth (Figure **F4**). Minor excursions in downhole temperature at 750 and 1100 mbsf suggest fluid influx into permeable fault zones. To vent at temperatures up to 116°C, the LCHF must mine fluid to several kilometers depth, based on inferences of circulation temperatures from fluid chemistry (Kelley et al., 2005; Allen and Seyfried, 2004, 2005; Foustoukos et al., 2008; Lang et al., 2012; Seyfried et al., 2015) and hydrothermal modeling (Titarenko and McCaig, 2016; Lowell, 2017). Close to the seafloor, the LCHF is localized by faulting (Denny et al., 2016); whether more diffuse or multichannel flow occurs at depth or whether there is shallow recharge and mixing is very important for the chemical and hence microbiological evolution of the system and therefore underpins all of our main objectives. New measurements of the thermal structure and fluid flow at depth at Site U1601 close to Lost City can provide important constraints on the hydrogeology of the Atlantis Massif.

2.6. Potential for abiotic organic synthesis

It is axiomatic that before life could begin on Earth or other worlds in the solar system, precursors of DNA, RNA, proteins, and other biologically relevant macromolecules must have been synthesized without biological intervention (Stüeken et al., 2013). The LCHF and Atlantis Massif have many features that make these synthesis reactions favorable; these locations have therefore been proposed as a model for the early Earth settings where prebiotic chemistry may have led to life (Kelley et al., 2002b; Martin et al., 2008). Serpentinization and abiotic organic synthesis reactions play a major role in generating H_2 and organic carbon molecules that are carried with fluids, including methane, ethane, propane, and small carboxylic acids such as formate (Kelley et al., 2001, 2005; Proskurowski et al., 2008; Lang et al., 2010, 2018; Wang et al., 2018; Klein et al., 2019). In samples recovered from nearby Hole U1309D, the amino acid tryptophan and additional carbonaceous material have been identified in association with iron-rich saponitic clays and proposed to be synthesized abiotically (Pisapia et al., 2018; Ménez et al., 2018).

A major driving factor for organic synthesis reactions is the production of H_2 in association with serpentinization reactions, which makes the reduction of CO_2 thermodynamically favorable (McCollom and Seewald, 2007, 2013). H_2 is likely to be generated from the reduction of H_2O in circumstances where the average Fe^{3+}/Fe^{2+} ratio of secondary minerals is higher than that of primary minerals (McCollom and Bach, 2009; Klein et al., 2009; Andreani et al., 2013). Experiments suggest generation rates are highest around 300°C (McCollom et al., 2016). Hydrogen has been detected in the water column widely across the Atlantis Massif, even in locations not associated with the focused circulation pathway of the LCHF (Lang et al., 2021).

Temperature and lithology are likely additional major controls on the type and abundance of organic compounds synthesized at the Atlantis Massif. Some reduced compounds, such as methane and short-chain alkanes, are believed to form through Fischer-Tropsch-type reactions at temperatures well above the known limit to life (Proskurowski et al., 2008; Wang et al., 2018; Klein et al., 2019), perhaps catalyzed by Fe-, Ni-, and Cr-bearing minerals (Foustoukos and Seyfried, 2004). These compounds may form at high temperature, trapped in fluid inclusions, and mobilize into circulating fluids when the system is at lower temperatures (Kelley and Früh-Green, 1999, 2001; Klein et al., 2019). In contrast, the formation of carboxylic acids, amino acids, and carbonaceous material likely proceeds at lower temperatures (<400°C), including within thermal regimes conducive to life (Lang et al., 2010; 2018; McDermott et al., 2015; Ménez et al., 2018; Klein et al., 2019; Andreani et al., 2023).

One goal of Expedition 399 was to examine abiotic organic synthesis in multiple settings spanning distinct thermal and geochemical regimes. Hole U1309D contains core material that never experienced temperatures lower than 140°C. Site U1601 was targeted as a location that could potentially recover material currently undergoing active serpentinization. In addition to recovering core material, we aimed to collect fluid samples from within the boreholes to provide critical insights into volatile and elemental distributions.

2.7. Thermal limits of life and the deep biosphere in the oceanic crust

To date, there is very little information about the existence of a deep biosphere in subseafloor serpentinizing systems. The warmest, highest pH domains of carbonate chimneys from the LCHF are dominated by a single clade of Lost City Methanosarcinales (Schrenk et al., 2004). Chimney exteriors are mixing zones between seawater and anoxic alkaline fluids and create gradients conducive to biochemical and microbial activity (Summit and Baross, 2001; McCollom and Seewald, 2007; Lang and Brazelton, 2020). DNA sequencing and lipid biomarker analyses have identified communities involved in H_2, CH_4, and sulfur cycling (Bradley et al., 2009; Brazelton and Baross, 2010; Brazelton et al., 2010, 2006; Méhay et al., 2013; Lang et al., 2018). A portion of the community actively cycles formate, an organic acid formed abiotically, deep in the circulation pathway (Lang et al., 2018; McGonigle et al., 2020).

Insights into the constraints on life in the subseafloor and the metabolic strategies that the small numbers of inhabitants employ can be gained in part through characterization of the endolithic communities. Distinguishing endemic microbial taxa from those introduced from seawater or contamination is a major challenge requiring multiple strategies to overcome (Kallmeyer, 2017; Sylvan et al., 2021; Pendleton et al., 2021). Nonetheless, the signatures of endolithic communities have been successfully identified from the subseafloor of the Atlantis Massif during both Expeditions 304 (Mason et al., 2010) and 357 (Motamedi et al., 2020; Goordial et al., 2021; Quéméneur et al., 2019) (Figure **F8**). Despite the widespread dominance of communities that cycle H_2 and CH_4 in the Lost City hydrothermal chimneys (Schrenk et al., 2004, 2013; Brazelton et al., 2006), genes associated with H_2 and CH_4 metabolisms were rare or absent in the Atlantis Massif subseafloor (Goordial et al., 2021). In general, the genes necessary for autotrophic carbon fixation pathways were rare, whereas those associated with heterotrophy were regularly identified (Quéméneur et al., 2019; Motamedi et al., 2020; Goordial et al., 2021). Enrichment experiments also primarily identified microorganisms that rely on heterotrophy (Quéméneur et al., 2019). Although early indications suggested that alkane degradation may be an important metabolic strategy in the gabbroic-dominated Hole U1309D (Mason et al., 2010), genes associated with alkane degradation were not detected in metagenomic studies of the more ultramafic Expedition 357 cores (Goordial et al., 2021). Using high-pressure incubations, a strictly anaerobic, mesophilic bacterium that

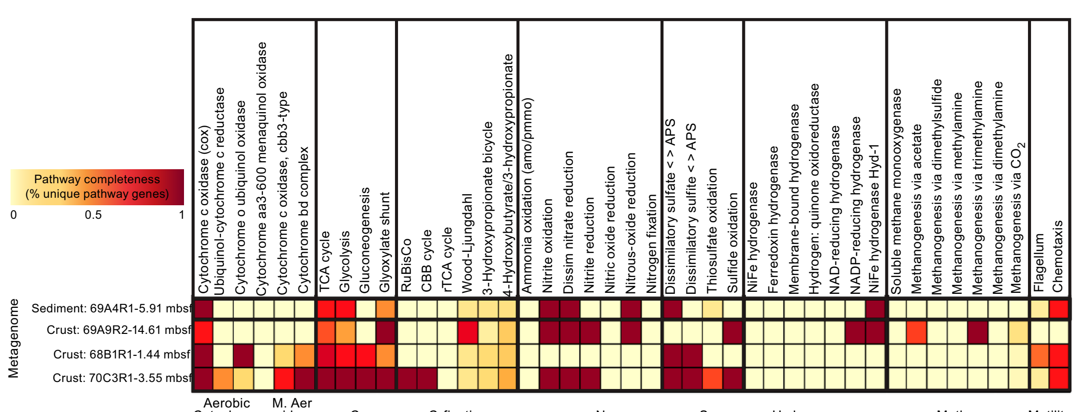

Figure F8. Metabolic potential of microbial communities isolated from subsurface sediments and crust from Atlantis Massif Expedition 357 samples based on metagenomes. Genes associated with autotrophy, including methanogenesis and methanotrophy, and alkane degradation were rare. Identified genes were associated with heterotrophy, aerobic carbon monoxide, and formate cycling. M. Aer oxidase = microaerobic cytochrome oxidase. From Goordial et al. (2021).

relies on fermentation of organic compounds for growth was successfully isolated from Expedition 357 Hole M0070C (Quéméneur et al., 2019).

Together, these data point to communities that are adapted to the Atlantis Massif subseafloor and quite distinct from those that inhabit the chimneys of the LCHF. Instead of capitalizing on the abundant thermodynamic energy available for autotrophy from the co-occurrence of H_2, CH_4, and SO_4 (Lang and Brazelton, 2020), they appear to rely instead on organic molecules that are either transported with seawater or synthesized in situ. Collecting deep samples from an actively serpentinizing system will allow us to explore the hypothesis that something (pH, low carbon dioxide availability, water availability, etc.) limits the biosphere in this subsurface system. It will also help us constrain the source of the organics that these communities require and determine whether they consume the abiotic organic molecules created as a result of serpentinization reactions.

3. Scientific objectives

The Atlantis Massif is one of the best studied near-ridge sites in the ocean floor; this allows our objectives to be driven by process and hypothesis rather than exploration. Operations during Expedition 399 were designed to address the following objectives.

3.1. Objective 1: characterizing the life cycle of an oceanic core complex and the links among igneous, metamorphic, structural, and fluid flow processes

Previous work summarized above shows that the massif is <2.0 My old and has been exposed by detachment faulting. A full range of processes including partial melting, intrusion of gabbros and melt-rock reaction, alteration and hydration by seawater over a wide range of temperatures, and deformation both within the detachment fault zone and at greater depths have occurred over this short time interval. This includes structure rotation by ~45° during the faulting process. The new data and samples collected as part of the expedition can provide insights into these ancient processes recorded in the rocks. In turn, fluid sampling and borehole temperature measurements can constrain the current thermal and hydrological structure of the massif and ongoing processes of fluid-rock interaction.

3.2. Objective 2: accessing the chemical kitchen that preceded the appearance of life on Earth

Environments that are actively serpentinizing have been proposed as potential locations for the origin and evolution of early life because water-rock reactions produce alkaline conditions that are favorable for prebiotic chemistry, H_2 that can drive the reduction of CO_2 to organic molecules, and gradients of redox and pH that promote biochemical reactions (Martin and Russell, 2006; Sojo et al., 2016). A consensus is emerging that serpentinization-related reactions play a major role in generating H_2, CH_4, short-chain hydrocarbons, and organic acids, and possibly even amino acids, and reduced carbonaceous material (Kelley and Früh-Green, 1999; Proskurowski et al., 2008; McCollom and Bach, 2009; McCollom and Seewald, 2013; Klein et al., 2013, 2019; Lang et al., 2010, 2018, 2021; McDermott et al., 2015; Ménez et al., 2018; Andreani et al., 2023). These compounds can become mobilized and available for microbial activity at lower temperatures around vent systems such as the LCHF, potentially the type of location where life evolved on the early Earth (Kelley et al., 2002a). The geochemical signatures of modern serpentinizing systems can provide important insights to the ancient processes that may have occurred, but modern overprints such as reactions with oxygen and active microbial communities obscure signals.

An open question is what the rates of serpentinization, hydrogen generation, and organic synthesis may be. A major goal of the expedition was to link abundances of H_2 and organic molecules with the physical, chemical, and temporal conditions that lead to their synthesis. A second major goal was to leave both the deepened Hole U1309D and the new peridotite-hosted hole at Site U1601 in a condition such that future expeditions could relog them for temperature and conduct fluid sampling.

3.3. Objective 3: characterize the deep biosphere and limits for life in the Atlantis Massif, in particular the impact of lithologic substrate, porosity, permeability, temperature, fluid chemistry, and reactive gradients

Results from shallow (<16.4 mbsf) coring on the southern wall during Expedition 357 indicate that the crustal subseafloor at the Atlantis Massif is a very low biomass ecosystem (Figure **F9**) compared to other crustal subsurface systems (Früh-Green et al., 2018). However, the depth of coring may not have been sufficient to intersect with large fluid flux pathways. Sampling for microbiological studies during Expedition 357, and during Expeditions 304 and 305 where low cell counts were also noted from Hole U1309D, did not specifically target the porous and permeable zones most likely to contain more substantial biomass. Despite low biomass, communities adapted to in situ conditions have been identified in recovered core material, including successful enrichment cultures (Mason et al., 2010; Quéméneur et al., 2019; Motamedi et al., 2020; Goordial et al., 2021). A target for Expedition 399 was to preferentially sample zones of higher porosity and permeability to test whether these regimes are associated with higher cell abundances. The highest cell counts recovered from Expedition 357 were adjacent to highly chloritized gabbro with relict reaction porosity that was infilled with chlorite down to conditions of <100°C (McCaig et al., 2022). Increased porosity, a less alkaline local fluid, or chemical gradients between serpentinite and gabbro may have promoted microbial growth. A major aim of drilling at Site U1601 was to recover samples that are similarly vuggy or in zones with mixed lithology or fluid chemistry.

The thermal structure of the Atlantis Massif offers a unique opportunity to study the temperature limits of a deep life in a crustal system because fluid temperatures in Hole U1309D (Figure **F4**) were expected to cross both the known upper thermal limit for life in laboratory cultures (122°C) and the lower suspected temperature limit (~80°–90°C) for life in energy-limited subsurface sedimentary systems (Heuer et al., 2020). Because many portions of the Atlantis Massif subseafloor are not energy limited, evidence of active life may be present even at the higher thermal limits only previously reached in laboratory cultures.

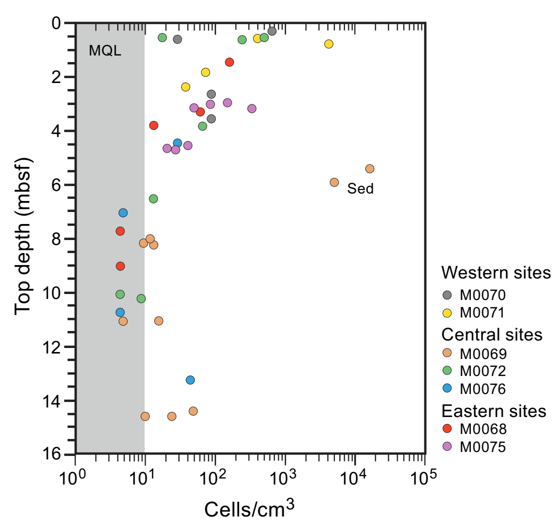

Figure F9. Cell counts from interior portions of whole-round cores, Expedition 357. Shaded area = minimum quantification limit (MQL) of 9.8 cells/cm^3. Sediment (Sed) samples from Site M0069 have higher cell counts than other samples from similar depths. Cell counts are generally low; serpentinites at base of Hole M0069A are deepest samples with significant cell counts. From Früh-Green et al. (2018). Reprinted from Lithos (v. 323), Früh-Green et al., "Magmatism, serpentinization and life: insights through drilling the Atlantis Massif (IODP Expedition 357)," pages 137–155, Copyright (2018), with permission from Elsevier.

4. Site summaries

4.1. Site U1309

4.1.1. Background and objectives

4.1.1.1. Previous drilling at Site U1309

Site U1309 is located on the central dome of Atlantis Massif, 14–15 km west of the median valley axis of the Mid-Atlantic Ridge, and ~5 km north of the LCHF (see **Background and objectives** in the Site U1309 chapter [McCaig et al., 2025]). The seafloor is interpreted to be a gently sloping, corrugated detachment fault surface (Figures **F1**, **F2**). The site was established during Expeditions 304 and 305 in 2004–2005, when the two main Holes U1309B and U1309D were drilled as well as five shallow and failed holes (Blackman, Ildefonse, John, Ohara, Miller, MacLeod, and the Expedition 304/305 Scientists, 2006; Blackman et al., 2011).

Expedition 304 established a hard rock reentry system comprising 25 m of 13⅜ inch casing in Hole U1309D using a hammer drill. During that operation, 4.5 m of casing was left protruding from the seafloor and a reentry cone was successfully dropped onto the casing. The hole was then deepened to 131 mbsf. After carrying out operations at Sites U1310 and U1311, Hole U1309D was deepened to 401 mbsf and logged. Expedition 305 followed directly after Expedition 304 and deepened Hole U1309D to 1415 mbsf in two stages, with logging runs in the middle and at the end of coring. Hole U1309D was reentered and logged during Expedition 340T in 2012 and had remained undisturbed from 25 February 2012 until operations during Expedition 399.

Hole U1309D sampled a continuous sequence of gabbroic rocks including troctolite and olivine-rich troctolite, olivine gabbros, oxide gabbros, and rare leucocratic intrusions (Figure **F4**). A few minor screens of mantle harzburgite are present in the upper 300 m of the section. Diabase/basalt intrusions with chilled margins form ~40% of the top 120 m of the sequence, with rare occurrences at greater depths. Many igneous contacts are present within the section, with units varying from centimeters to tens of meters in thickness (John et al., 2009). More evolved units generally (but not always) intrude into more primitive units.

Crystal-plastic deformation is restricted to narrow zones in the section, mainly above 300 mbsf. Cataclasis and fault breccia are present in several strands in the uppermost 80 m of the section, a fault zone at ~160 mbsf, and a prominent 6 m thick fault zone at 744–750 mbsf within a damage zone from 742 to 761 mbsf (Michibayashi et al., 2008; John et al., 2009). A crystal-plastic deformation zone at 1100 mbsf is suggested by temperature logging and has a weak signal in the core.

Alteration is most extensive in the upper 300 m of the section, where clinopyroxene is usually at least partly altered to amphibole (hornblende and actinolite) in both gabbro and diabase. In olivine-bearing rocks, coronitic tremolite and chlorite form at the expense of olivine and plagioclase. Below 300 mbsf, this reaction only goes to completion around faults and gabbro contacts (Nozaka and Fryer, 2011) and rodingitization of plagioclase to prehnite ± hydrogarnet driven by serpentinization of olivine is seen (Frost et al., 2008). The latest reactions and veins contain saponite and zeolites (Nozaka et al., 2008) and may be forming in near ambient conditions.

Temperature logging occurred at the end of Expedition 305 and again during Expedition 340T, 7 y later (Blackman, Ildefonse, John, Ohara, Miller, MacLeod, and the Expedition 304/305 Scientists, 2006; Expedition 340T Scientists, 2012). During Expedition 305, the temperature gradient was strongly affected by drilling, with a steep rise in the lowest part of the hole and a maximum temperature of 118.9°C at 1415 mbsf. During Expedition 340T, the temperature profile in the borehole water was assumed to have equilibrated with the rock and reached 146.2°C at 1405 mbsf. Below ~750 mbsf, the temperature gradient is linear, and a conductive regime is inferred. Above 750 mbsf, the temperature profile is curved, suggesting slow downward movement of fluid in the rock mass (Blackman et al., 2014). Small excursions in temperature, seen at ~750 and 1100 mbsf, are inferred to be the result of influx of colder fluid.

Samples for microbiology were taken from a range of lithologies and depths during Expeditions 304 and 305 (Blackman, Ildefonse, John, Ohara, Miller, MacLeod, and the Expedition 304/305 Scientists, 2006; Mason et al., 2010). Cell counts were below detection limit (<10^3 cells/cm^3 rock). Microbial diversity was assessed using cloning and sequencing, terminal restriction fragment length polymorphism, and a microarray for metabolic genes (GeoChip). The low-diversity microbial communities consisted of lineages closely related to bacteria from hydrocarbon-dominated environments and known hydrocarbon degraders (Mason et al., 2010).

Figure **F1** (Harding et al., 2016) shows the most recent processing of the seismic data collected more than 20 y ago and used to select the location for Site U1309. Seismic velocities increase with depth, with velocities of 7 km/s below 1000 mbsf, consistent with fresh gabbro (Blackman et al., 2011). At higher levels, lower velocities reflect alteration of gabbro and increased fracturing consistent with slow fluid circulation inferred from the temperature profile (above). Physical properties measured on the ship and logging data including VSPs collected during Expeditions 305 and 340T are consistent with the lithologies collected and were used in processing the full waveform inversion model shown in Figure **F1** (Harding et al., 2016).

4.1.2. Objectives of Site U1309 revisit

Expedition 399 objectives at Site U1309 were the following:

- To sample fluids and obtain temperature data in the undisturbed borehole and study geochemistry and microbiology of fluids at temperatures above and below the current known limit of life;
- To mill out a caliper arm lost during Expedition 340T and believed to be in the bottom of Hole U1309D, leaving the hole in good condition for further operations;
- To deepen the hole by ~650 m to reach temperatures of ~220°C, where active serpentinization reactions might be occurring and where increasing amounts of mantle rock might be expected within the gabbroic sequence; and
- To drill an additional single-bit hole at Site U1309 with the aim of sampling zones of fault-induced and reaction porosity for microbiology that were not collected during Expedition 304.

Although our first two objectives were realized, Hole U1309D was only deepened by 83 m and a new shallow hole was not drilled. In light of the unexpectedly good results at Site U1601, the Science Party decided that achieving a deep hole in peridotite (the original aim of Expeditions 304 and 305) at Site U1601 should be prioritized.

4.1.3. Principal results

4.1.3.1. Igneous petrology

Deepening Hole U1309D from 1415 to 1489 mbsf during Expedition 399 recovered predominantly gabbroic rocks (Figure **F10**): gabbro (27%), olivine-bearing gabbro (59%), and olivine gabbro (12%), with small proportions of crosscutting diorite and diabase (1% and 2%, respectively). As was observed for the 1415 mbsf interval drilled during Expeditions 304 and 305, olivine-bearing rocks are abundant in the newly drilled interval. However, the proportion of gabbro below 1415

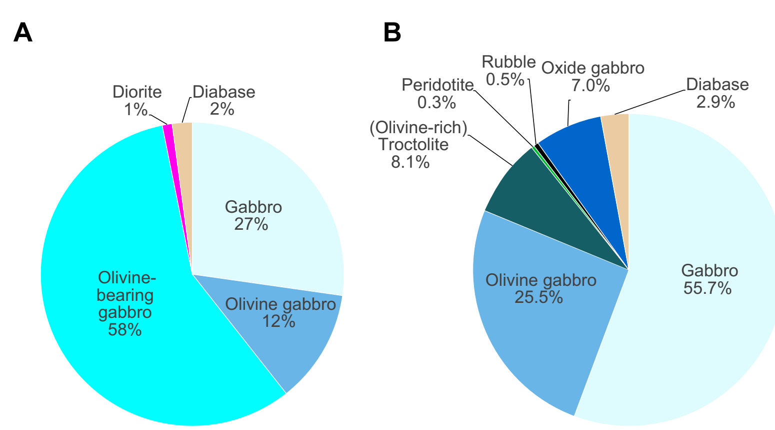

Figure F10. Recovered lithology, Hole U1309D. A. 1415–1498 mbsf (Expedition 399) B. 0–1415 mbsf (Expedition 304/305).

mbsf is significantly higher and the proportion of olivine gabbro is significantly lower than above that interval. In addition, many of the rock types recovered at shallower levels in Hole U1309D were not recovered during Expedition 399, including ultramafic rocks, troctolite, tonalite, trondhjemite, and oxide gabbros.

The main recovered gabbro body has internal gradational contacts between rocks with different grain sizes, mineral modes, and textures (subophitic to ophitic to poikilitic), indicating that the different subunits form part of a continuum of crystallization within a single plutonic body rather than representing discrete intrusions. In general, olivine was first to crystallize, followed by plagioclase and clinopyroxene. Crystallization continued as melt compositions evolved. This is evidenced by the common presence of zoning in plagioclase and late-stage crystallization of orthopyroxene. The general lack of the characteristic assemblage of amphibole + Fe-Ti oxide indicates that this late-stage melt did not generally evolve to the point of oxide saturation.

Following accretion of the gabbroic units, two stages of additional magmatism occurred. First, diorite veins intruded, forming sutured and reactive contacts. The sutured and reactive nature of the contacts indicate that intrusion occurred when the gabbroic rocks were still at elevated temperatures. The final igneous activity is marked by the diabase dikes. Their chilled margins attest to intrusion in a relatively cold environment. Furthermore, the thin section observations of entrainment of hydrothermally altered microxenoliths indicate that at least some diabase intrusions occurred after the host gabbroic rocks had already suffered hydrothermal alteration.

4.1.3.2. Alteration petrology

Gabbroic rocks recovered from Hole U1309D during Expedition 399 show low degrees of alteration (<20 vol% secondary replacement; Figure **F11**). An exceptionally high extent of alteration occurs at intervals where localized alteration associated with cataclastic deformation, prominent hydrothermal or magmatic veining, and patchy bleaching took place. Alteration minerals appear to have formed under static conditions, except for amphibole formation associated with localized deformation in cataclastic zones.

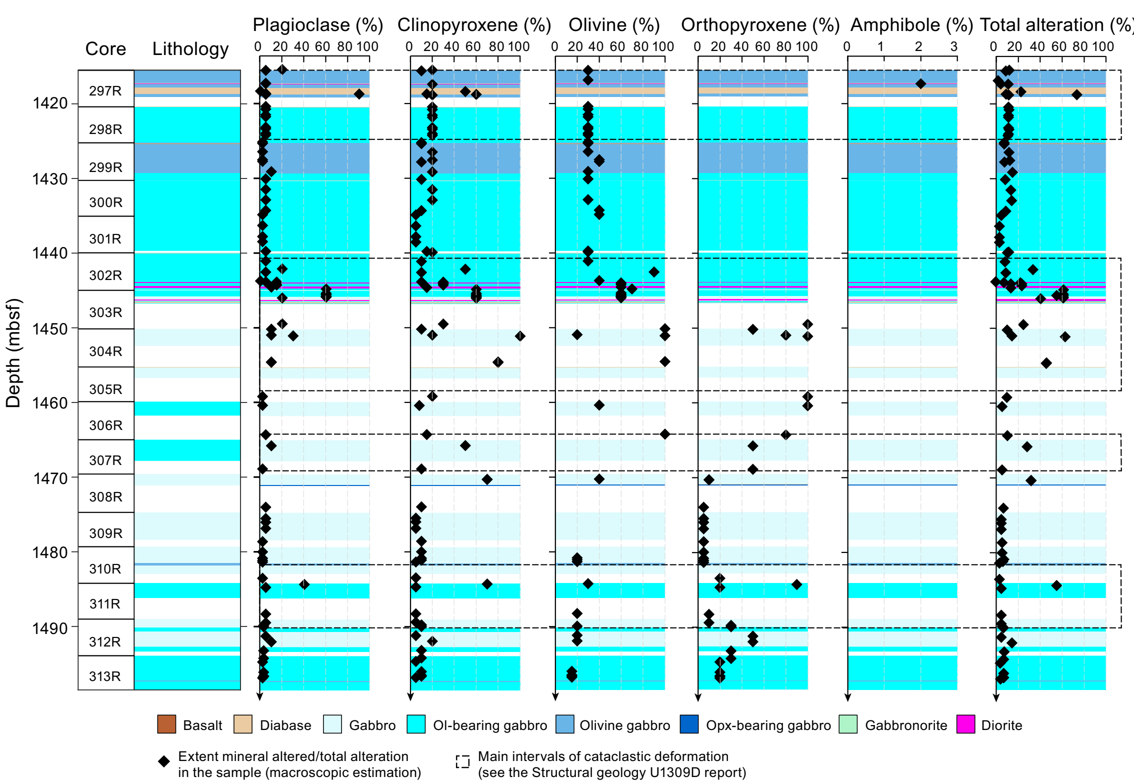

Figure F11. Downhole variation of percentage of alteration extent of each mineral and percentage of total alteration intensity in gabbroic rocks, Hole U1309D below 1415 mbsf. See Figure F4 for total alteration intensity from 0 to 1415 mbsf (Expedition 304/305). Ol = olivine, Opx = orthopyroxene.

Zeolite, amphibole, chlorite, and composite amphibole-chlorite veins frequently occur throughout cores without systematic downhole distribution. Crosscutting relationships of veins indicate a sequence of generation stages from older to younger: (1) magmatic veins; (2) amphibole, chlorite, or amphibole + chlorite veins; and (3) prehnite + carbonate and zeolite veins.

The observations of mineral assemblages, microscopic textures, fluid inclusions, and crosscutting relationships between the alteration assemblages and between hydrothermal veins indicate that sequential alteration and deformation took place at conditions ranging from amphibolite through greenschist to subgreenschist facies conditions. Each primary mineral in gabbroic rocks is partially replaced by secondary minerals at grain boundaries, along microcracks, or cleavage surfaces. In some cases, particularly in proximity to hydrothermal veins, complete replacement yields pseudomorphs after primary minerals. Olivine is replaced by distinct mineral assemblages composed of serpentine + oxide/sulfide, talc + sulfide/oxide, clay + oxide/sulfide, or amphibole + oxide + chlorite or a combination of one or more of these assemblages. Fluid inclusions formed during healing of fluid-filled fractures are locally abundant in olivine and plagioclase. Clinopyroxene and orthopyroxene are altered to amphibole, chlorite, and/or talc. Plagioclase is altered to chlorite, amphibole, secondary plagioclase, prehnite, and zeolite.

The interplay among magmatic processes, deformation, and fluid flow is recorded in alteration mineral assemblages of lower crustal lithologies from Hole U1309D. The findings presented here are consistent with those from Expeditions 304/305 and provide additional constraints on alteration processes to 1498 mbsf.

4.1.3.3. Structural geology

Structural analysis of Cores 399-U1309D-297R through 313R (1415–1498 mbsf) recovered during Expedition 399 reflects a temporal and spatial overlap in magmatism and semibrittle to brittle deformation processes in the footwall of an oceanic detachment system.

Magmatic fabrics in the recovered gabbroic rocks are dominantly isotropic with grain size variations and rare diffuse contacts between grain size domains. Rare magmatic foliations, shown by shape-preferred orientation of plagioclase or pyroxene, have gentle to subvertical dips.

Rare crystal-plastic deformation was only observed microscopically. Gabbroic rocks that appear undeformed at the macroscale infrequently display very low strain crystal-plastic deformation (twinning and/or subgrains) in plagioclase. Localized fault rocks can display subgrain development and minor grain boundary bulging dynamic recrystallization in plagioclase related to brittle to semibrittle deformation of relict igneous plagioclase.

Brittle to semibrittle deformation is concentrated in two strands of a semibrittle shear zone between 1451 and 1460 mbsf (Sections 399-U1309D-304R-2 through 306R-1) and between 1464 and 1474 mbsf (Sections 307R-1 through 308R-1), with relatively undeformed rocks in sections above and below these intervals. The shear zones are characterized by brittle to semibrittle deformation over a significant range of intensities from fractures and microfaults, faults, and fault breccia to formation of zones of cataclasite and phyllonite. Microscopic analysis of high-intensity deformation zones shows localized plagioclase-amphibole cataclasite and amphibole phyllonite fault cores. Reverse shear sense was determined in rare cases where structural orientation was preserved in recovered intervals. Diabase dikes in some cases cut cataclastic zones (Figure **F12**).

The most abundant vein types include amphibole, chlorite, and zeolite veins and minor prehnite and carbonate veins, formed across a broad range in temperature. Crosscutting relationships and vein deformation record that amphibole and chlorite veins are pre-/syn- and postdeformational. Additionally, amphibole-chlorite alteration of fractured rocks is typically undeformed. Low-temperature zeolite, prehnite, and carbonate veins are undeformed and therefore postdate deformation. Collectively, the deformation mechanisms in plagioclase and amphibole, taken with crosscutting relations between deformation, alteration, and vein generation, demonstrate that semibrittle deformation occurred at lower amphibolite to greenschist facies conditions.

The cores reflect a down-temperature history from crystallization of gabbroic rocks, cooling with very limited deformation to lower amphibolite–upper greenschist facies conditions, followed by semibrittle deformation in a shear zone at lower amphibolite to greenschist facies conditions along shear planes with present-day dips of 10°–30°. Because the depth of the interval is 1415–1498 mbsf, it is unlikely that the reported semibrittle shear zone is directly related to the detachment fault exposed at the seafloor. The greenschist facies conditions of deformation suggest that Atlantis Massif continued to deform during the later stages of exhumation, followed by a phase of magmatism (diabase).

4.1.3.4. Geochemistry

Geochemical analyses were carried out on rock samples selected by the geochemistry and microbiology teams and fluids collected during the two separate water sampling campaigns. A total of 29 rock samples from Hole U1309D were analyzed for major and trace element concentrations and for volatile element concentrations. These samples comprised (a) 1 diabase, 1 leucocratic diorite, 3 olivine gabbro, and 15 gabbro (including 10 olivine-bearing gabbro) collected for rock geochemical studies and (b) 1 olivine gabbro sample and 8 olivine-bearing gabbro samples analyzed as part of an interdisciplinary study of rock samples collected primarily for microbiological studies.

The analyzed samples do not display systematic chemical variations with depth except for those associated with the crosscutting diabase at 1417.9 mbsf and leucocratic diorite at 1443.8 mbsf.

Expedition 399 olivine gabbros and gabbros have major and trace element compositions similar to those of the most primitive gabbros and the most evolved olivine gabbros recovered at Site U1309 during Expeditions 304 and 305. They overlap in composition and are characterized by high Mg# (74–80) and Ca# (73–82) and low TiO_2 concentrations (0.26–0.50 wt%). Except for some microbiology samples that have H_2O up to 2.17 wt%, they have low H_2O contents similar to Hole U1309D gabbroic rocks sampled below 850 mbsf. The presence of H_2O indicates the replacement of primary minerals by hydrous minerals during hydrothermal alteration and weathering. The major and trace element compositions of Expedition 399 olivine gabbros and gabbros provides no evidence of elemental remobilization associated with H_2O concentration variations, even for fluid mobile elements.

The analyzed leucocratic sample is from the felsic part of the diorite sample recovered at ~1444 mbsf. Its composition is that of an An_{45} plagioclase, and, except for Sr, an element typically enriched in plagioclase, it is depleted in almost all trace elements. In that respect, it differs significantly from the previously analyzed Site U1309 leucocratic veins and dikes that represented the most enriched end-members of the rocks recovered during Expeditions 304 and 305. The fine-grained diabase intruding the gabbroic rocks at 1417.9 mbsf has a basaltic composition characterized by high Mg# (69) and low TiO_2 concentrations (0.79 wt%). It represents one of the most primitive, depleted, and least altered basaltic intrusions of the MORB magmatic suite at Site U1309.

Based on their major and trace element compositions, Expedition 399 Hole U1309D diabase and gabbroic rocks form a coherent suite with the diabase, basalt, and gabbroic rocks sampled at the same site during Expeditions 304 and 305, indicating a cogenetic origin for these mafic rocks.

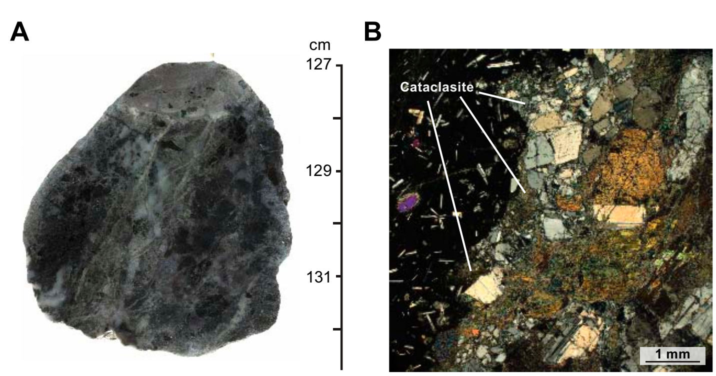

Figure F12. A. Diabase cutting fractured olivine-bearing gabbro (399-U1309D-303R-1, 126–132 cm). Diabase is at 127–128 cm. B. Chilled margin of undeformed diabase against zone of cataclasis in isotropic olivine gabbro (297R-2, 97–100 cm [TS22]; cross-polarized light).

In the initial fluid sampling campaign in Hole U1309D, the inaugural deployment of the Multi-Temperature Fluid Sampler (MTFS) successfully recovered fluids from four depths and the Kuster Flow-Through Sampler (KFTS) recovered fluids from an additional four depths. Both samplers returned with abundant solid material that was likely a mixture of drilling mud, cuttings from the borehole, bottom fill, and grease. The fluids appear to be a mixture of seawater, formation water, and a fluid that reacted with fill at the base of the hole. The second fluid sampling campaign, carried out 33 days after drilling operations ceased, collected an additional three KFTS samples with full volumes and three samples with incomplete recovery. The samplers did not return large amounts of solid material from these deployments, and the fluids were notably clearer. The geochemistry of the fluids are similar to the surface seawater used to flush the hole during drilling, with intrusion of deep seawater in the upper portion of the borehole. Below 600 mbsf, geochemical changes could indicate intrusion of formation fluids and/or reactions with rubble at the base of the borehole.

4.1.3.5. Microbiology

Microbiological investigations in Hole U1309D were designed to explore potential signs of recent or past life at extreme temperatures, in particular the shallowest rocks that may have been exposed to borehole water during the 18 y since Expedition 305. Microbiology samples were collected for traditional analyses such as cell counts, cultivation, and DNA sequencing, as well as organic geochemistry analyses intended to document the presence of organic compounds including lipids, organic acids, and amino acids. A total of nine microbiology whole-round samples were collected from Cores 399-U1309D-297R through 313R. Eight of the samples are olivine-bearing gabbro, and one sample is olivine gabbro.

Each of the nine samples was rinsed, photographed, and separated into exterior and interior sections according to our standard methodology. Perfluorocarbon tracer (PFT) levels in the interior sections of all nine samples were below detection or at very low levels (maximum of 0.1 ppb). In contrast, PFT was detectable in the exterior shavings of all microbiology whole-round samples except one, ranging from trace levels to 22 ppb. The consistent reduction of PFT levels from exterior shavings to interior zones affirms the efficacy of our procedures for limiting contamination into the interior zones of the core samples.

Subsamples from each of the nine samples were collected for cell counts, DNA sequencing, lipid characterization, and organic carbon analyses. Subsamples for single-cell activity assays were collected from six of the nine samples. Stable isotope tracer experiments were conducted with four of the samples. Subsamples for virus counts, enrichment cultivations, and scanning electron microscope imaging were collected from the first five samples. High-pressure cultivation experiments were conducted with subsamples collected from Cores 399-U1309D-297R and 298R.

Water samples collected with Niskin bottles, the MTFS, and the KFTS were subsampled for microbiological analyses intended to characterize the extent, diversity, and activity of microbial communities within Hole U1309D. Subsamples for cell counts and single-cell activity assays were collected from all four of the high-volume MTFS samples (Bottles 1, 2, 4, and 5) and all KFTS and Niskin samples. In addition, MTFS Bottle 2 was subsampled for virus counts, enrichment cultivations, high-pressure cultivations, and stable isotope tracer experiments. Water from MTFS Bottle 4 (260 mL), the three KFTS bottles (250 mL each), and all Niskin bottles (3–5 L) were filtered through a 0.2 µm Sterivex filter cartridge intended for DNA sequencing.

4.1.3.6. Petrophysics

The petrophysical properties of gabbro in Hole U1309D were characterized through natural gamma radiation (NGR), magnetic susceptibility, and gamma ray attenuation (GRA) density measurements on whole-round cores from Cores 399-U1309D-297R through 313R (1415–1498 mbsf). Discrete measurements were completed on cubes and included wet mass, dry mass, and dry volume for the calculation of density and porosity and *P*-wave velocity. Core pieces from section halves were selected for thermal conductivity measurements. Downhole temperature logs were completed. No other petrophysical logging was attempted in this hole.

Bulk density from whole-round measurements ranges 2.6–2.9 g/cm^3 and generally increases with depth. Some intervals deviate from this trend, including a general downhole decrease in density in

Cores 399-U1309D-302R through 303R (1441–1445 mbsf) that is also mirrored in the grain density measured on discrete cube samples.

A total of 31 discrete cube samples were analyzed. Grain density ranges 2.–3.0 g/cm^3 (average = 2.9 ± 0.1 g/cm^3). Grain density and bulk density generally increase with depth. Grain density is negatively correlated with porosity; porosity generally decreases with depth. Porosity ranges 0.5%–2% (average = 1.27 ± 0.79%). The highest porosity is measured in Cores 399-U1309D-302R through 305R (1441.2–1455.0 mbsf), which also includes an altered felsic dike that has a grain density of 2.55 g/cm^3 and a porosity of 5%.

P-wave velocity was measured on 30 discrete cube samples (1 diabase, 3 olivine gabbro, and 26 gabbro) along the three principal directions *x, y*, and *z* in the core reference frame (CRF). The average *P*-wave velocity of the three-axis on each sample ranges 4965–5895 m/s (average = 5476.0 m/s), and the apparent anisotropy of *P*-wave velocity ranges 4.1%–7.0%.

Magnetic susceptibility is relatively low, reflecting a relatively low proportion of magnetite in these rocks. Pass-through loop magnetic susceptibility (MSL) is typically less than 500 instrument units (IU), and point magnetic susceptibility (MSP) is typically less than 1000 IU. The highest values for MSL (~1500 IU) and MSP (~6500 IU) are in Section 399-U1309D-311R-1, indicating more abundant magnetite.

NGR is very low with most values <0.5 counts/s. Thermal conductivity was measured on 17 archive-half core pieces >10 cm in length. Samples of representative lithologies for the hole were measured. Values for all pieces range 2.14–2.63 W/(m·K) with a mean of 2.35 ± 0.14 W/(m·K). No obvious trend with depth or lithology exists.

Borehole fluid temperatures were measured in Hole U1309D prior to coring. The best results were recorded with the first run down the hole, with the Elevated Temperature Borehole Sensor (ETBS) attached to the MTFS. Values for the entire borehole during the down run range from 6.7°C at the seafloor to 139.6°C near the bottom of the hole. The resulting profile shows slight curvature in the upper ~580 mbsf, transitions into a more linear gradient deeper than 580 mbsf, and continues linearly to the bottom of the hole. The profile in the deeper half of the hole indicates a gradient of ~114°C/km. The temperature profile is very similar to that recorded during Expedition 340T, indicating no significant changes in hydrological or heat flow regime in the last 11 y.

4.1.3.7. Paleomagnetism

Remanence measurements were made on archive section halves from Hole U1309D, adding to the breadth of knowledge for the preexisting hole. These measurements generated 6281 new measurement points downhole. The mean natural remanent magnetization (NRM) inclination was determined to be −25.7° ± 12°. Stronger alternating field (AF) steps of 10–15 mT shift and narrow the distribution toward the expected geocentric axial dipole (GAD) value of −49°. At the AF step of 50 mT, the mean inclination became −34.4°. This shallower inclination value relative to the expected value is consistent with previous work on the hole. The cause for shallowing was interpreted to be the result of tectonic rotation.

Archive section half data were complemented by discrete sample measurements. Both paleomagnetic and physical properties cube samples were analyzed using AF demagnetization, thermal demagnetization, isothermal remanent magnetization (IRM) acquisition, and IRM backfield methods. Additionally, paleomagnetic cube samples were pretreated with liquid nitrogen dunking as a way of reducing the drilling overprint. Multiple remanence directions were recorded, but the direction of the most coercive components was consistent with the mean inclination direction, as put forth by the archive section half analysis. The bulk remanence of these rocks is carried by magnetite. The intensity of magnetic remanence varies downhole, ranging 0.02–3.81 A/m (mean = 0.90 A/m), indicating varying distributions of magnetite. Results from the isothermal remanence experiments provide evidence for predominantly multidomain and minimal single-domain magnetite grain populations.

Anisotropy of magnetic susceptibility (AMS) data indicate predominantly oblate magnetic fabrics. The clustering of the shortest magnetic axis (K_{min}) around the vertical indicates that the direction of magnetic flow was horizontal. The degree of anisotropy (P_j) averages 1.121 ± 0.075 (n = 50) with low and high values ranging 1.029–1.424. The average value of P_j indicates that most susceptibility tensors are moderately anisotropic but significantly higher degrees of anisotropy are noted in many coarse-grained gabbroic samples.

4.2. Site U1601

4.2.1. Background and objectives

Site U1601 is located on a flat region near the southern wall at the top of the Atlantis Massif at a water depth of 850 m (see **Background and objectives** in the Site U1601 chapter [Lang et al., 2025b]). Mass wasting along the southern edge of the massif has created steep cliffs that expose a 3000 m cross section of the internal structure. The southern wall is predominantly composed of variably altered peridotite with intermittent mafic plutonic intrusions (Blackman et al., 2002; Schroeder and John, 2004; Früh-Green et al., 2003, 2018; Boschi et al., 2006; Karson et al., 2006).

The location of Site U1601 was chosen in part based on the success of drilling in this region during Expedition 357. The central Sites M0069A, M0072B, and M0076B were drilled to 12.4–16.4 mbsf, with recoveries ranging 52%–75% (Früh-Green et al., 2017). Recovered cores contained diverse lithologies with upper layers that included calcareous sediment, basalt, and dolerite. Serpentinized harzburgite was recovered in the deeper sections of all three boreholes (Früh-Green et al., 2017), and water column concentrations of H_2 were elevated to ~40 nM above these locations (Lang et al., 2021), suggesting that deeper drilling may encounter rocks undergoing active serpentinization. It was also hoped that a hole at this site would recover a complete section through the detachment fault zone, suggested to be ~100 m thick. Several of the shallow holes of Expedition 357 recovered fault rocks including cataclasites and talc-tremolite-chlorite schists. Thus, a hole located near one of the central sites could address many of the primary goals of the expedition.

A location adjacent to Hole M0069A was specifically targeted because it had some of the best recovery during Expedition 357. It was also the location of the deepest serpentinite sample subjected to microbiological analyses (14.6 mbsf), revealing cell densities of 10–24 cells/cm^3 (Früh-Green et al., 2018). Genes from putative indigenous subsurface organisms were identified from Core 357-M0069A-92R (Goordial et al., 2021) and other nearby drilling locations (Motamedi et al., 2020).

The scientific objectives for Site U1601 were initially intended to complement the goal of deepening Hole U1309D by targeting a zone with thermal and geochemical conditions more conducive to microbial activity and the potential abiotic synthesis of organic molecules. Recovering a section through the 50–100 m thick detachment fault zone (Schroeder and John, 2004; Karson et al., 2006) would also allow for a more complete characterization of the core complex. The high recovery and rapid progress while drilling Hole U1601C provided an opportunity to expand the initial objectives to those originally intended for Hole U1309D. In addition, the unexpected depth of Hole U1601C opened the possibility to identify large-scale structural, igneous, and alteration relationships across a long section of serpentinized peridotite and to access material representative of the hydrothermal reaction zone supplying fluids to the Lost City hydrothermal system (Lissenberg et al., 2024).

4.2.2. Objectives of operations at Site U1601

1. Drill a section of serpentinized ultramafic crust to a depth of 200 mbsf, the initial goal of Expedition 357, to provide a complete section through the oceanic detachment fault zone into less deformed rocks below.
2. Characterize the abundances and distributions of microorganisms and carbon associated with ultramafic rocks at temperatures more conducive to biological activity and the abiotic formation of organic molecules than those at the bottom of Hole U1309D.
3. Collect wireline logging and paleomagnetic data to reconstruct subseafloor data in regions of incomplete recovery, to allow reorientation of the core, and to provide temperature profiles for future hydrogeologic modeling efforts.

4. Conduct a continuous and consistent survey of abundances and distributions of microorganisms and carbon across a long downcore profile to document the changes as temperatures and geochemical conditions become more challenging to life.
5. Identify potential signs of fluid flow and characterize formation fluid geochemistry.
6. Characterize the igneous, structural, geochemical, and alteration characteristics of a largely continuous section of abyssal peridotite to document lithology, mineralogy, bulk-rock compositions, structural evolution, and indications of hydrothermal alteration

Objectives 1–3 represent our initial expedition goals for this site, and Objectives 4–6 emerged as Hole U1601C reached greater depths than expected.

4.2.3. Principal results

4.2.3.1. Igneous petrology

The primary igneous and mantle lithologies are summarized here without regard to changes induced by deformation and alteration. Drilling at Site U1601 recovered in situ sections of mantle rocks with subordinate igneous intrusions. Combined, Holes U1601A and U1601C are dominated by serpentinized peridotites, with 56% harzburgite, 9% orthopyroxene-bearing dunite, and 3% dunite (Figure **F13**). Gabbroic lithologies constitute approximately one third of the total and have a range of scales, from millimeter-sized veins to bodies tens of meters in size. Diorite, diabase plus basalt, and ultramafic veins are rare (<1% total).

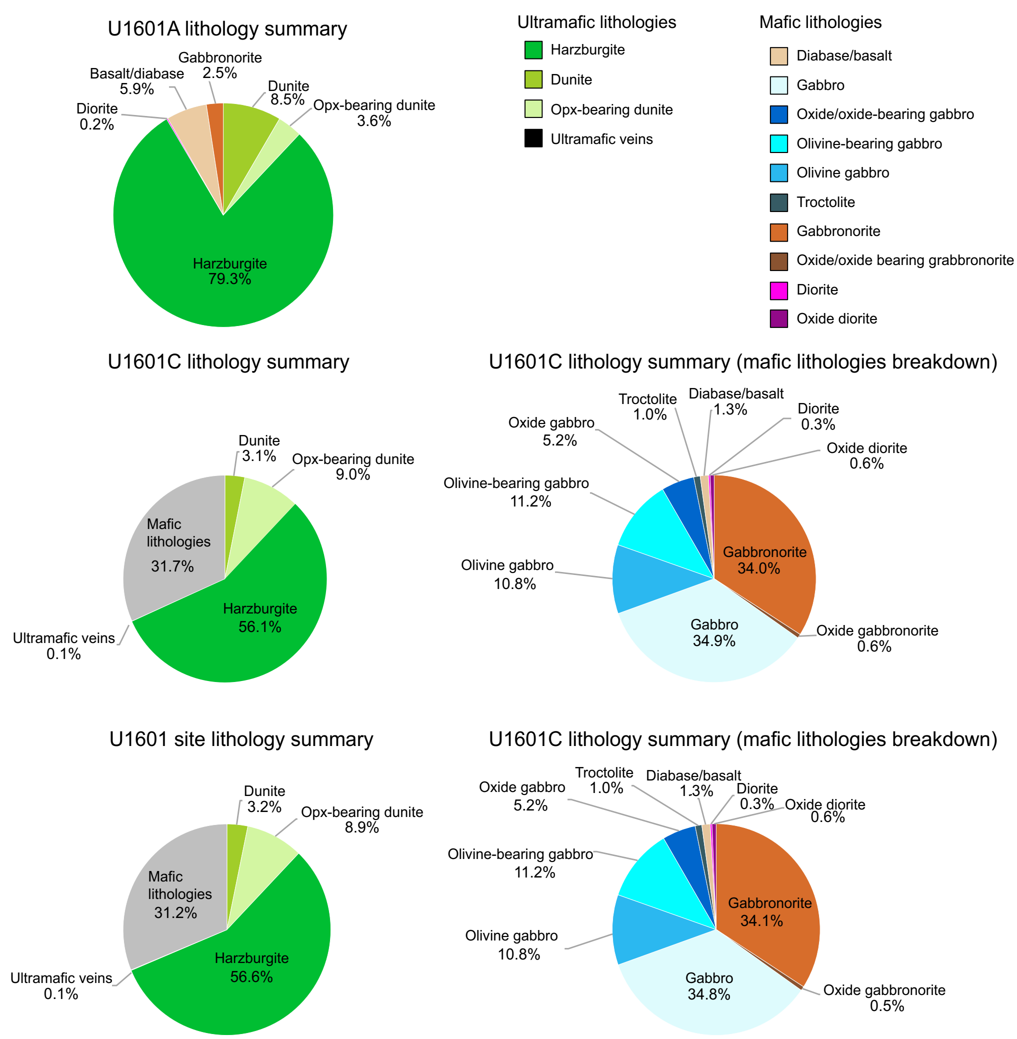

Figure F13. Lithologic percentages of recovered cores, Site U1601. Final lithologic distributions may require updating once thin sections are available. Opx = orthopyroxene.

4.2.3.1.1. Hole U1601A

Hole U1601A cores are mostly peridotites (harzburgite to dunite) with subordinate basalt, gabbronorite, and diorite (Figure **F14**). Six lithologic units were defined within the sequence, primarily based on changes in lithology. Subunits were defined in some of these units where mineral modes changed or where veins crosscut a unit.

The uppermost unit is microcrystalline aphyric basalt with filled vesicles (Subunit 1A) and segregation veins (Subunit 1B). Below the basalt is a series of peridotites with primary textures severely overprinted by alteration and deformation. The uppermost peridotite unit (Unit 2) is a highly altered and weathered harzburgite. The unit below is a dunite (Unit 3) with patches and trails of Cr-spinel. The dunite is mostly pyroxene poor (Subunit 3A) but grades into an interval of orthopyroxene-bearing dunite (Subunit 3B). The dunite is underlain by two narrow intervals of highly deformed and altered gabbronorite (Unit 4), separated by a single pebble of dunite (Subunit 4B).

The rest of Hole U1601A is dominated by harzburgite. At shallow levels, it is highly altered and weathered (Unit 5) and becomes slightly fresher below 27.7 mbsf (Unit 6). Unit 6 peridotite has variable proportions of pyroxene and associated variations in texture. Orthopyroxene proportions vary at the scale of a few to tens of centimeters, ranging 10%–25%. Locally, orthopyroxene proportions are below 10% and the harzburgite grades into orthopyroxene-bearing dunite (Subunit 6D). From Section 399-U1601A-10R-1 (49 mbsf), two different orthopyroxene morphologies are present, granular and interstitial, indicative of a multistage petrogenetic history (Subunit 6E). Clinopyroxene is relatively rare (<3%) and mostly confined to the upper 23 m of the unit. The Unit 6 harzburgite contains a narrow interval of deformed gabbronorite (Subunit 6B) and is crosscut by a centimeter-wide diorite vein (Subunit 6C).

Hole U1601A was drilled in the general footprint of Expedition 357, and the igneous stratigraphy of this hole is similar to nearby Hole M0069A. The aphyric and microcrystalline nature of the basalt recovered at the top of Hole U1601A resembles the diabase found in Hole M0069A. Like Hole M0069A, a series of harzburgite and dunite was recovered below the basalt/diabase, with the dunite containing Cr-spinel. No gabbroic rocks were recovered in Hole M0069A, although narrow (tens of centimeters) metagabbro and oxide gabbro intervals were observed in Holes M0072B and M0076B located within ~600 m of Hole U1601A. Further, in contrast to the three Expedition 357 central sites (Holes M0069A, M0072B, and M0076B) no talc-amphibole-chlorite schists or breccias were recovered in Hole U1601A. Whether this is a genuine geologic difference or it relates to the low recovery (~8%) during drilling the shallowest sections of Hole U1601A is uncertain.

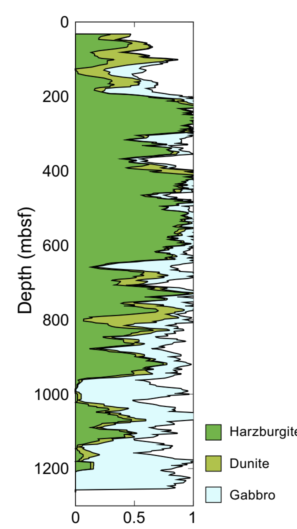

Figure F14. Running average for harzburgites, dunites (including orthopyroxene-bearing dunites), and gabbroic rocks recovered using 10 m bin size and 2 m step size between each iteration, Hole U1601C. Final lithologic distributions may require updating once thin sections are available.

4.2.3.1.2. Hole U1601C

Recovery of cores in Hole U1601C began below casing at 23 mbsf and terminated at 1268 mbsf. Unit 1 of this hole consists of microcrystalline to aphyric basalt. A long in situ section of mantle rocks with subordinate igneous intrusions is below. Unit 2 comprises the primary peridotite lithologies. Subunit names for these lithologies are primarily based on the relative proportions of olivine and orthopyroxene because the recovered mantle lithologies are dominated by clinopyroxene poor varieties. Subunit 2A is harzburgite, Subunit 2B is orthopyroxene-bearing dunite, and Subunit 2C is dunite. Each gabbroic body encountered has a unit name unless nearby intervals have similar magmatic features even if separated by another unit (e.g., an interval of peridotite).

The distribution of the various rock types in the section is uneven (Figure **F13**). In the uppermost 180 m, dunite is relatively abundant. Gabbroic intrusions are relatively common between ~120 and ~195 mbsf. Between 200 and 640 mbsf, the section is dominated by harzburgite (Figure **F14**) with rare dunite and gabbro. The proportion of gabbroic rocks gradually increases again from ~640 mbsf, and gabbros are particularly prevalent below ~950 mbsf.

Orthopyroxene varies in abundance, grain size, and grain shape in the peridotites. These variations occur on a decimeter to several-hundred-meter scale. Orthopyroxene is less abundant at 0–200 mbsf and 800–1200 mbsf and more abundant around 230, 410, and 750 mbsf. Orthopyroxene abundances and grain sizes correlate, with smaller grain sizes (generally 2–5 mm) in orthopyroxene-bearing dunite and larger grain sizes of 5–8 mm in the most orthopyroxene-rich (>25% orthopyroxene) harzburgite. In addition, grain size of orthopyroxene is smaller in dunite than in harzburgite (Figure **F15**). As was observed in Hole U1601A, both granular and interstitial orthopyroxene grains have been identified. Clinopyroxene is frequently absent, and where present it is generally rare. Based on thin-section descriptions, clinopyroxene abundance averages 1%. Cr-spinel is nearly ubiquitous in the peridotites. Most samples have significantly less than 1% Cr-spinel, although it reaches higher proportions (1%–3%) in some dunitic rocks.

Minor amounts of other ultramafic lithologies were recovered in the upper 600 m of Hole U1601C. These rocks show a range of modal abundances, ranging from websterite and olivine websterite to orthopyroxenite and wehrlite. They are typically found as veins in olivine-rich peridotite hosts.

Gabbroic bodies are found throughout Hole U1601C and are particularly concentrated toward the bottom of the hole (>950 mbsf). In total, we recorded 438 intrusive bodies, comprising 301 units. Most individual gabbroic bodies are millimeter- to centimeter-sized veins (Figure **F16**), with progressively fewer intrusions in the 10 cm–1 m, 1–10 m, and >10 m categories. By volume (as measured on the section half surface and uncorrected for unit dips), approximately three quarters of the gabbro bodies are >1 m thick and approximately one quarter of the gabbro bodies are thicker than 10 m (Figure **F17**).

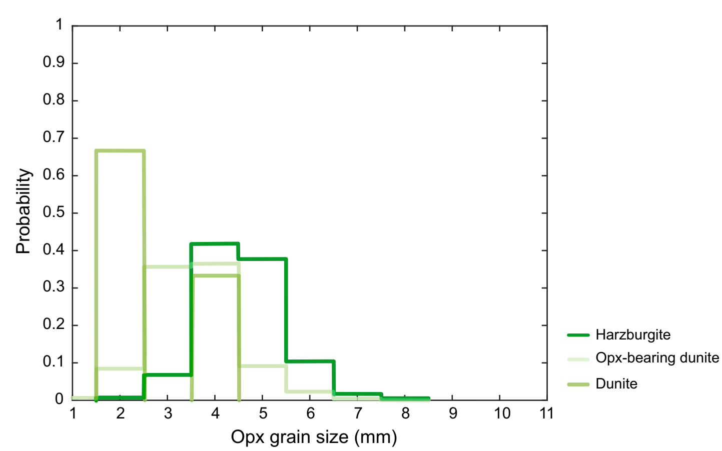

Figure F15. Orthopyroxene (Opx) grain size distribution in peridotites, Hole U1601C. Note progressive decrease in grain size between harzburgite, orthopyroxene-bearing dunite, and dunite.

Lithologically, the gabbroic rocks are dominated by gabbro and gabbronorite with lesser olivine gabbro, oxide gabbro/gabbronorite, and troctolite. Gabbro and gabbronorite have a wide range of thicknesses, whereas troctolite is present only as components of larger gabbroic bodies (0.1–10 m). Oxide gabbro and gabbronorite typically occur in centimeter- to decimeter-scale intervals within gabbroic bodies with less abundant oxide. Texturally, the gabbroic rocks in Hole U1601C are dominated by coarse average grain sizes and granular textures.

Contacts between gabbroic rocks (veins aside) and their host peridotites are generally sutured, and gabbroic rocks are commonly separated from the surrounding peridotite by a centimeter-scale zone of troctolite or olivine gabbro (Figure **F18**). Some gabbros have multicentimeter long clinopyroxene crystals at the contacts with peridotites.

Other minor lithologies in Hole U1601C are diorite and diabase. Diorite occurs as minor components in larger gabbroic bodies and is usually composed of plagioclase and hornblende, commonly with oxides. The diorite has textures suggesting that it intruded into and reacted with gabbro after the gabbro was largely or entirely crystallized. Diabase is present as 3 cm to 2.1 m dikes crosscutting gabbros.

4.2.3.2. Alteration petrology

4.2.3.2.1. Hole U1601A

Hole U1601A recovered a range of rock types including basalt, gabbroic rocks, and serpentinized peridotites, all of which show evidence of fluid-rock interaction. Minor amounts of fine-grained aphyric basalt recovered in the upper parts of Hole U1601A are characterized by heterogeneous

Figure F16. Cut surface showing discrete gabbronorite vein in harzburgite, Hole U1601C.

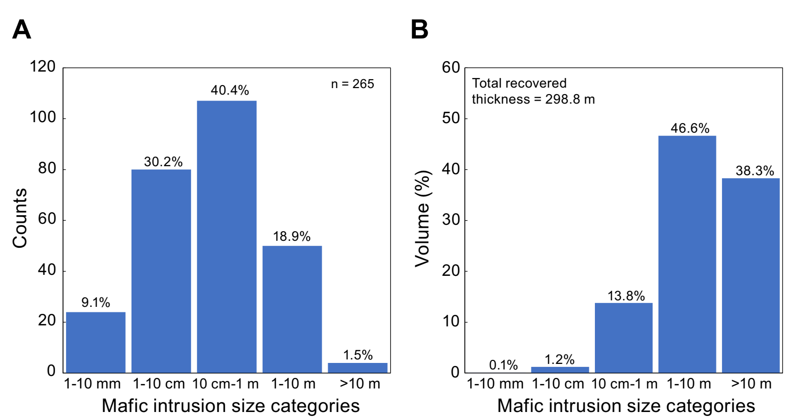

Figure F17. A, B. Intrusion size as function of lithology for gabbroic rocks, Hole U1601C. Note that histograms count size of intrusions in which given lithologies occur, but intrusions do not have to be composed entirely of this lithology to be included (e.g., troctolites and oxide gabbros occur preferentially in larger intrusions but typically only form minor component of them).

patchy alteration that is moderate on average. Serpentinized harzburgite and dunite are highly altered, with degrees of alteration ranging around 70%–100%. On average, harzburgite is less altered than dunite. In serpentinized peridotites, olivine is highly altered to serpentine, magnetite, and traces of sulfides or alloy(s), as well as locally iowaite after brucite (Figure **F19**), and orthopyroxene is partially to completely altered to serpentine and talc, forming bastite. No systematic downhole variation of the total extent of whole-rock serpentinization is observed in Hole U1601A, nor of the extent of alteration of individual minerals, except for orthopyroxene, which is less altered in the upper parts of Hole U1601A. Scarce magmatic intrusions of gabbroic composition are less altered than their peridotite hosts, with extents of alteration ranging ~5%–96% in individual intervals and thin sections.

In addition, several types of veins are present in serpentinized peridotites, basalt, and gabbroic rocks in Hole U1601A. Basalt contains chlorite-epidote, monomineralic chlorite, and epidote veins, amphibole-chlorite and minor zeolite-chlorite, secondary clay-chlorite, and oxide-carbonate veins. In serpentinized peridotites, the dominant vein types include serpentine-magnetite, serpen-

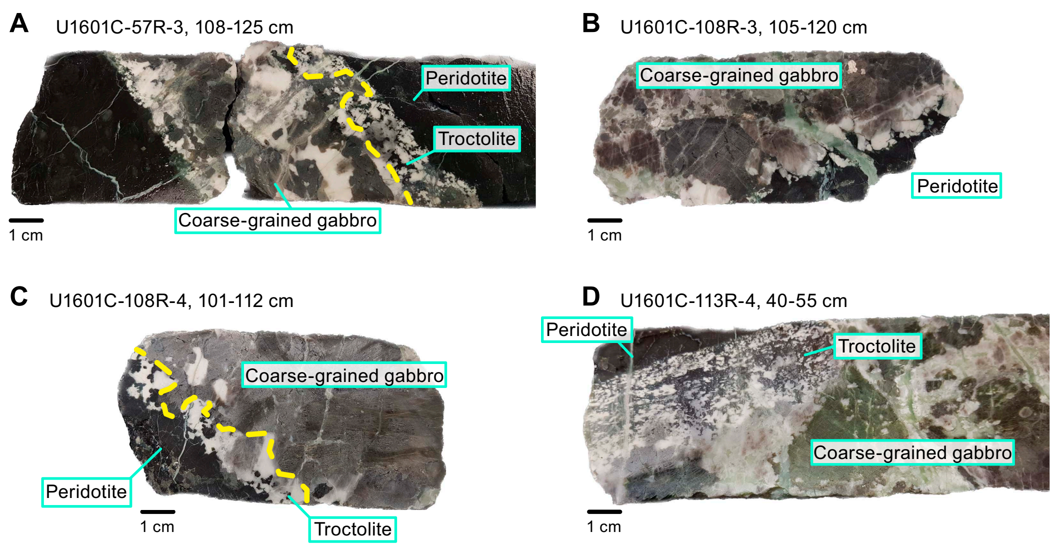

Figure F18. Troctolite contacts between coarse-grained gabbros and peridotites, Hole U1601C. A. Troctolite is present along contacts on both sides between gabbro intrusion and peridotite, with one side thicker than the other. Note interstitial habit of olivine in troctolite. B. Relatively thin troctolite contact between gabbro and peridotite, with euhedral plagioclase crystal growing across contact. C. Granular olivine in mixed olivine gabbro to troctolite contact between coarse-grained gabbro and peridotite. D. Thick troctolite with olivine-rich areas at gabbro-peridotite contact.

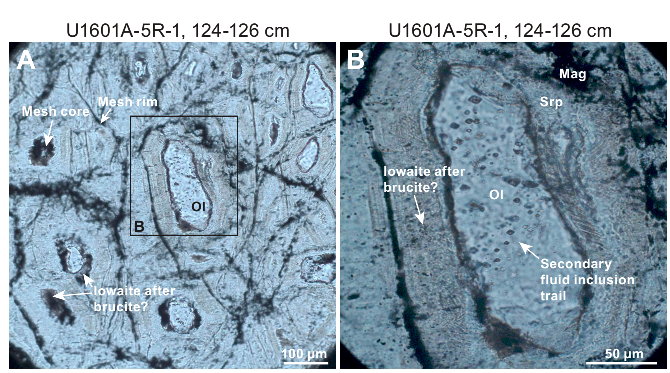

Figure F19. Mesh interiors and olivine relicts in serpentinized dunite, Hole U1601A (TS6; plane-polarized light). A. Typical serpentine, brucite, and iowaite mesh texture after olivine (ol); mesh rims are composed of magnetite-serpentine veins. Presence of iowaite in sample was confirmed by XRD, location is inferred. B. Enlargement showing olivine relicts containing trails of secondary fluid inclusions. srp = serpentine, mag = magnetite.

tine, and carbonate-serpentine and rare oxide veins. A few carbonate-brucite veins were also identified.

4.2.3.2.2. Hole U1601C

In Hole U1601C, gabbroic rocks are slightly (3%–20% alteration of the total rock volume) to highly (51%–99% alteration of the total rock volume) altered, whereas throughout the drill hole serpentinized harzburgite, orthopyroxene-rich dunite and dunite are moderately (21%–50%) to completely (100%) altered. The estimated extent of serpentinization of peridotites is highly variable on the meter to thin section scale and ranges 40%–100%, which is consistent with the extent of serpentinization estimated from downhole densities. In serpentinized peridotites, olivine is highly altered to serpentine, magnetite, and traces of sulfides or alloy(s), as well as locally brucite and iowaite, which forms as a replacement product of brucite. Orthopyroxene is altered to serpentine forming bastites, in which talc and/or chlorite can be locally abundant. Clinopyroxene shows the lowest degrees of alteration and is replaced by amphibole and/or serpentine. No downhole variation of serpentinization degrees could be observed; rather, alteration degrees are higher in both peridotites and gabbroic rocks where they are in contact with each other. Using modal abundances of the igneous minerals of harzburgite, orthopyroxene-bearing dunite, and dunite and their degree of serpentinization estimated based on thin section observations, we calculate an average degree of serpentinization of around 88% for Hole U1601C. In shallow intervals, magnetite is locally oxidized to reddish brown iron oxide and iron oxyhydroxide minerals, indicative of less reducing conditions near the seafloor (Klein et al., 2017). At greater depths, magnetite seems less altered. Locally, in zones where serpentinized peridotite is juxtaposed with gabbroic lithologies, disseminated sulfide minerals were observed in the mesh. In addition, serpentinized peridotites are cut by several types of veins including hydrothermally overprinted magmatic veins, serpentine ± magnetite, carbonate ± sulfide veins, and sulfide veins. The serpentine veins comprise an earlier generation composed of antigorite and/or lizardite and magnetite and a later generation composed of chrysotile or picrolite, suggesting that several serpentinization events occurred (Figure **F20**).

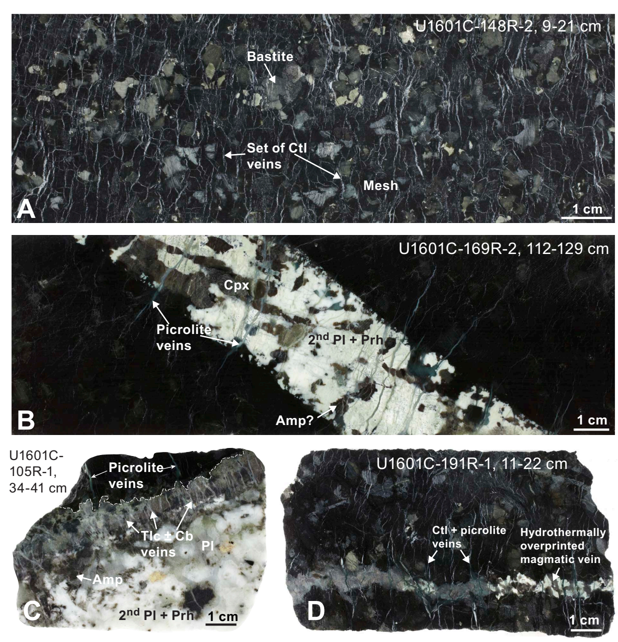

Figure F20. Main vein type occurrences in serpentinized peridotites and at serpentinized peridotite/gabbroic rocks contact, Hole U1601C. Scale bars = 1 cm. A. Set of white, fibrous to massive, subparallel horizontal transgranular to locally paragranular chrysotile (Ctl) veins cutting serpentinized harzburgite. B. Hydrothermally overprinted magmatic vein of clinopyroxene (Cpx), amphibole (Amp)?, prehnite (Prh), and secondary plagioclase (2nd Pl) cut by set of green massive picrolite veins. C. Contact between serpentinized peridotite and altered gabbro. Set of talc (Tlc)-carbonate (Cb) veins branches at contact and further continues in gabbro but not in serpentinite. A few picrolite veins cut through serpentinite and grade to prehnite veins when propagating in gabbro. D. Hydrothermally overprinted magmatic vein cut by set of composite chrysotile-picrolite veins. Picrolite vanishes away from magmatic vein.

In Hole U1601C gabbro, gabbronorite, olivine gabbro, troctolite, and oxide gabbro were recovered. Gabbroic rocks are more extensively altered in intervals with a high degree of ductile and brittle deformation, high density of hydrothermal veins, and at contacts with serpentinite. The main types of veins include amphibole, chlorite, talc, carbonate, and zeolite veins. Brown amphibole coexisting with recrystallized clinopyroxene in deformed gabbroic rocks is possibly of magmatic origin. Localized static alteration associated with hydrothermal veining resulted in the replacement of primary minerals by secondary ones (i.e., olivine by amphibole, talc, serpentine, magnetite, clay minerals, and sulfides; pyroxene by amphibole, talc, chlorite, and/or clay minerals; and plagioclase by secondary plagioclase, chlorite, prehnite, and zeolite).

Throughout Hole U1601C, highly altered (rodingite-like) veins and metasomatized zones along the contact between mafic and ultramafic rocks were observed (Figure **F21**). These show highly variable mineral assemblages from almost monomineralic chlorite to amphibole-chlorite ± talc-rich lithologies to amphibole-prehnite-talc-±(hydro-)garnet-rich assemblages. These lithologies document extensive mass transfer between mafic and ultramafic lithologies at variable temperatures between <200° and 400°C.

The observations of mineral assemblages, microscopic textures, fluid inclusions, and crosscutting relationships of the alteration assemblages and hydrothermal veins indicate that sequential alteration and deformation of rocks at Site U1601 took place at conditions ranging from amphibolite through greenschist to subgreenschist facies. Macroscopic (millimeter scale or above) reaction porosity was recognized in a number of thin sections of altered gabbros from Site U1601, and per-

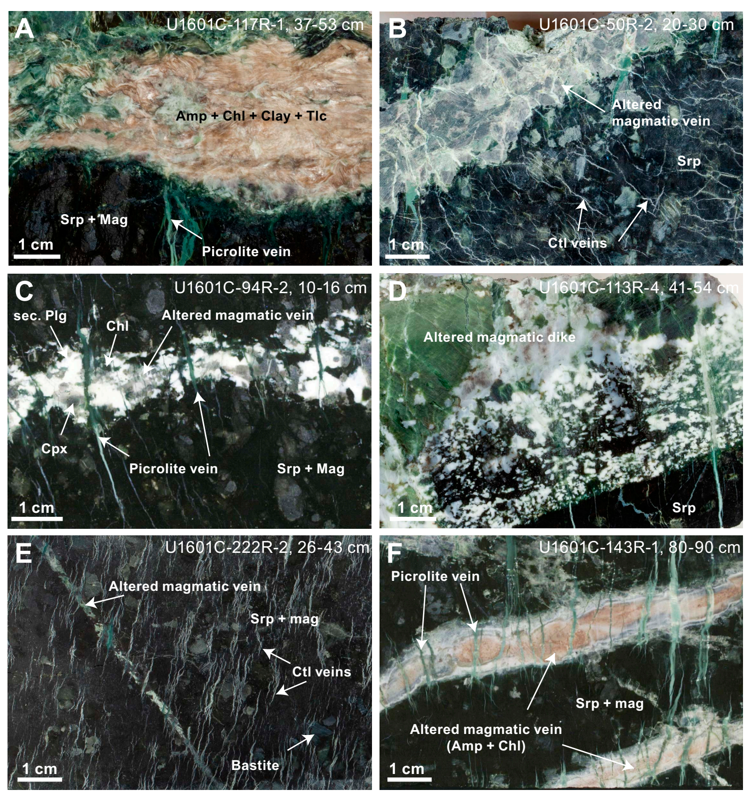

Figure F21. Diversity of hydrothermally altered magmatic veins intruding into serpentinized peridotite, Hole U1601C. A. Metasomatic reaction zone comprised of amphibole (Amp), chlorite (Chl), clay, and talc (Tlc) formed by mass transfer between ultramafic and mafic lithologies. B. Hydrothermally altered magmatic vein in serpentinite (Srp) cut by picrolite and chrysotile (Ctl) veins. C. Altered magmatic vein of prehnite, secondary prehnite, and chlorite cut by green picrolite veins. D. Highly altered magmatic dike intruding into serpentinized peridotite. E. Thin (2–3 mm wide) vein cutting serpentinized peridotite. Green picrolite veins cut the altered magmatic vein and white, fibrous chrysotile veins cut serpentine + magnetite (mag) mesh texture and bastites. F. Hydrothermally altered magmatic vein of amphibole and chlorite cutting serpentinized peridotite. Altered magmatic vein is cut by green picrolite veins. Plg = plagioclase.

meability enhanced by dissolution of minerals may have facilitated fluid access and hydration reactions along gabbro/peridotite contacts.

4.2.3.3. Structural geology

The structural evolution of the 1.2 km section cored at Site U1601 varies with recovered rock type. Holes U1601A and U1601C show similar structural geology in their overlapping intervals between 0 and 55 mbsf; both are characterized by rare intervals of crystal-plastic and brittle deformation. Below 55 mbsf, all structural observations are recorded from Hole U1601C, as summarized below.

Magmatic veins are common throughout Hole U1601C, cutting both harzburgite and older host gabbro and showing variable dips that steepen with depth. Thicker intervals of gabbro display rare magmatic foliations, with 75% of measured fabrics restricted to more evolved gabbro and gabbronorite. Isotropic grain size layering/domains are common with modal layering less common. Domain contacts are typically diffuse and irregular in shape.

Mantle fabrics and serpentine foliation hosted in peridotite vary in intensity with subhorizontal to moderate dips, barring the interval 630–800 mbsf, where steep mantle fabrics and contacts are noted. In most cases, mantle fabrics and serpentine foliation are misoriented with respect to each other.

Crystal-plastic deformation is limited in extent above 630 mbsf. Below 630 mbsf, protomylonitic to ultramylonitic crystal-plastic deformation is localized in five 25–50 m thick high-strain shear zones and one zone of distributed deformation separated by zones of little deformation. A total of 95% of crystal-plastic deformation occurs in gabbroic rocks, and it is typically concentrated adjacent to gabbro/peridotite contacts with contact-subparallel dips (Figure **F22**). Macroscopically, undeformed gabbroic rocks commonly display minor dynamic recrystallization of plagioclase. Mylonitic gabbro samples are dominated by dynamic recrystallization of plagioclase and to a lesser extent, pyroxene and amphibole. All five high-strain zones display reverse sense deformation. Shear Zones 1 (630–675 mbsf), 3 (950–975 mbsf), and 5 (1125–1150 mbsf) also show local normal shear sense. Where present, normal sense mylonitic foliation is steeper (>50°) than reverse sense fabrics; steep mylonitic fabrics overprinted by late shallow mylonitic fabrics are infrequently observed. Rare diabase/microgabbro intervals display both pre- and postdeformation relationships with crystal-plastic fabrics, some of which are crystal-plastically deformed; others are crosscutting mylonitic fabrics. Amphibole and chlorite veins cut mylonitic fabrics. Microstructural fabrics, mineral assemblages, and crosscutting relationships suggest mylonitization occurred at granulite through amphibolite facies conditions.

Sparse occurrences of brittle deformation (fracturing, brecciation, and cataclasis) overprint each crystal-plastic shear zone as well as some intervals within the low strain zones, including the interval 420–580 mbsf, and is commonly associated with hydrothermal veins. Total strain accommodated by brittle deformation is low. Slickenfibers record dominantly reverse sense shear. Brecciated diabase is observed.

Hydrothermal veins are more common between 0 and 300 mbsf and between 400 and 750 mbsf, with variable dips. Thin white chrysotile veins are a common feature of the serpentinized harzburgite, and typically mimic the orientation of local serpentine foliation. Talc veins observed in gabbroic intervals, particularly at gabbro/peridotite contacts, are commonly sheared but can both cut mylonitic foliation in gabbro or be undeformed.

Fault rocks clearly linked to detachment faulting were not recovered at Site U1601, although some fabrics in gabbroic rocks might be formed during related footwall deformation. In particular, no talc-tremolite-chlorite schists, which were recovered from multiple Expedition 357 holes (Früh-Green et al., 2016, 2017), were recovered. Poor recovery in Hole U1601A and casing to ~22 mbsf in Hole U1601C means that unrecovered fault rocks cannot be ruled out in the top 25 m of Site U1601. The 100 m thick detachment shear zone inferred from submersible studies (Karson et al., 2006) is not supported by our findings.

4.2.3.4. Geochemistry

Whole-rock chemical analyses (major and trace element concentrations, total carbon and hydrogen, and inorganic carbon) were performed on 255 samples from Site U1601 for geochemical and microbiological studies. In Hole U1601A, 7 serpentinized peridotites and 1 diabase were collected as geochemistry samples and 7 serpentinized peridotites and 1 basalt were collected for microbiology studies. In Hole U1601C, 144 serpentinized peridotites and serpentine veins, 44 variously altered gabbroic rocks, and 3 diabase and crosscutting carbonate veins were sampled as microbiology samples and 24 serpentinized peridotites, 20 gabbroic rocks, and 5 basalt and diabases were selected as geochemistry samples.

Microbiology samples have highly variable compositions compared to geochemistry samples. This is likely the result of a sampling bias toward collecting material hypothesized to host more abundant microbial biomass including (1) more altered samples with higher prevalence of veins and/or (2) rocks with mixed mafic–ultramafic lithologies.

The composition of the serpentinized peridotites overlaps the field of refractory serpentinized peridotites previously collected during Leg 209 at the 15°20′ Fracture Zone (also known as the Fifteen Twenty Fracture Zone [FTFZ]; Kelemen, Kikawa, Miller, et al., 2004; Godard et al., 2008). These compositions suggest that Site U1601 peridotites underwent high degrees of melt

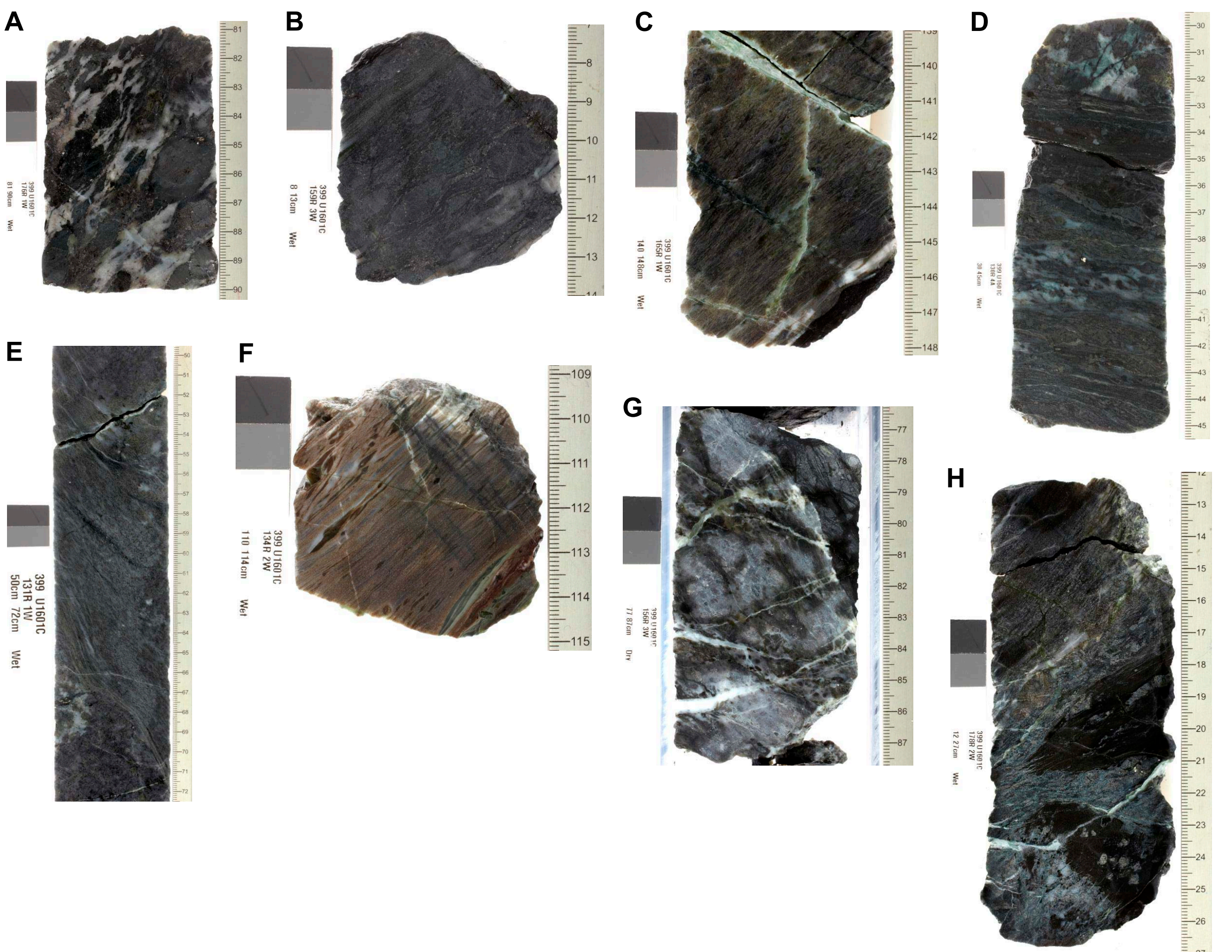

Figure F22. Wet images. A. Gabbroic protomylonite (399-U1601C-176R-1, 81–90 cm). B. Oxide-gabbro protomylonite (159R-3, 8–13 cm). C. Gabbroic mylonite to ultramylonite in contact peridotite (dark brown, bottom right), reverse shear sense; undeformed talc ± carbonate ± prehnite veins cut mylonite (176R-1, 81–90 cm). D. Oxide-gabbro with protomylonitic, mylonitic, and ultramylonitic domains, controlled by variability of protolith grain size and/or lithology (130R-4, 30–45 cm). E. Gabbroic mylonitic to ultramylonite discrete shear zone, normal shear sense (131R-1, 50–72 cm). F. Gabbroic ultramylonite (134R-2, 100–114 cm; unoriented). G. Irregular sheared contacts between mylonitic gabbroic rock (gray) and protomylonitic peridotite (dark brown); alteration veins cut mylonitic fabric (178R-2, 12–27 cm). H. Sheared contact between protomylonitic gabbroic rock (gray) and protomylonitic peridotite (dark brown-gray, top left); green-white talc ± carbonate ± prehnite alteration and veins overprint and cut mylonitic fabric (156R-3, 77–78 cm).

extraction. There is chemical evidence of extensive interaction with MORB-type melts (iron enrichment) in several samples, mostly dunites.

The composition of Site U1601 gabbroic rocks overlaps with the full range of Site U1309 gabbroic rocks. The most evolved gabbros were recovered at the bottom of Hole U1601C. With one exception, the gabbros below 650 mbsf are the least altered of those sampled for geochemistry at Sites U1309 and U1601.

The serpentinized peridotites, gabbroic rocks, and other lithologies collected at Site U1601 contain variable amounts of carbon, mostly hosted in Ca-carbonates, in contrast to the low abundance of carbon in rock samples recovered at Site U1309. The highest carbon values are found in the microbiology samples.

Fluids were collected from Hole U1601C in two ways. First, fluids collected from the series of KFTS runs shortly after logging operations were a mixture of the fresh drill water used to flush the hole, seawater, and possibly formation fluids. Second, eight cores were returned during drilling with significant volumes of fluid due to obstructions between the core and the plastic liner. The geochemistry of these samples was similar to the surface seawater used to flush the hole during drilling, with some samples that had slightly higher pH values. Borehole fluids collected with the KFTS contained detectable H_2 and CH_4 concentrations that increased with depth. Small fluid volumes that were recovered from the core catcher of most cores contained highly variable H_2 concentrations that did not increase or decrease with depth.

4.2.3.5. Microbiology

Microbiological investigations at Site U1601 were intended to explore the potential for life in the shallow subsurface of the Atlantis Massif at a site where serpentinized rocks were expected to be prevalent. Initial observations of cores from Hole U1601A were consistent with this goal. The surprising depth of Hole U1601C provided the unexpected opportunity to document the distribution of life through >1.2 km of the Atlantis Massif, possibly spanning environmental conditions from highly favorable to too extreme for life. Microbiology samples were collected for traditional analyses such as cell counts, cultivation, and DNA sequencing, as well as organic geochemistry analyses intended to document the presence of organic compounds including lipids, organic acids, and amino acids.

A total of eight microbiology whole-round samples were collected from Cores 399-U1601A-2R through 12R. Six of these samples are serpentinized harzburgite plus one diabase and one serpentinized dunite.

A total of 191 microbiology whole-round samples were collected from 172 different cores from Hole U1601C. These samples were chosen with the goal of assembling a sample collection that is balanced with respect to apparent biological potential and geologic representation while avoiding pieces that are geologically unique. Most samples are serpentinized harzburgite (60%), followed by serpentinized orthopyroxene-bearing dunite (14%), gabbro (12%), and serpentinized dunite (5%).

PFT assays were conducted with (1) samples of loose rubble collected during the core shake out, (2) chiseled shavings of the exteriors of microbiology whole-round samples, and (3) crushed interior zones after the exteriors were removed by chiseling. PFT levels in loose rubble samples were in the range of 1–10 ppb in most samples and reached 10–25 ppb in 20 samples. A few extreme outliers up to 257 ppb were the result of accidental increases in the rate of PFT delivery during drilling. The fairly consistent and high levels of PFT in loose rubble samples confirmed the successful delivery of PFT during drilling. In contrast, PFT was absent or present at only trace levels in nearly all samples of crushed interiors. These results indicate that surface contamination, as measured by PFT, was largely removed from the interior samples.

The 191 microbiology whole-round samples from Hole U1601C were subsampled for up to 16 different microbiological and biogeochemical analyses, including microscopy (synchrotron-based microscopy, scanning electron microscopy, and counts of cells and viral-like particles), sorting of single cells, and analyses of DNA, lipids, and organic compounds. A wide range of cultivation experiments were also conducted, including incubations of crushed interiors in filter-sterilized seawater (157 samples), enrichment incubations (88 samples with different temperatures and nutrients), high-pressure incubations (5 samples), and stable isotope tracer experiments (33 samples).

Samples of borehole water from Hole U1601C were collected with the KFTS to characterize the extent, diversity, and activity of microbial communities within Hole U1601C. In addition, small volumes of fluids collected from the core catcher and analyzed for H_2 concentrations were also used for microbiological analyses, including single-cell activity and sorting experiments and DNA sequencing.

4.2.3.6. Petrophysics

The petrophysical properties of rocks at Site U1601 were characterized through measurements on whole-round cores, including measurements of NGR, magnetic susceptibility, and GRA bulk density. Discrete measurements were completed on rock cubes and cuttings of microbiology samples and included wet mass, dry mass, dry volume, and *P*-wave velocity. Bulk density, grain density, and porosity were calculated from the mass and volume measurements. *P*-wave measurements were also completed on archive half pieces when rock cube samples were not available in Hole U1601C. Additionally, archive section half core pieces >10 cm in length were selected for thermal conductivity measurements. Downhole temperature logs were completed in Hole U1601C. A total of five wireline logging tool strings were deployed in Hole U1601C. The diameter of the borehole from caliper measurements is quite regular and is close to the bit size (9.73 inch) with a few larger diameter intervals. The hole is deviated a total of 10° from vertical in a northeast direction at the maximum logging depth (~1060 mbsf).

4.2.3.6.1. Density and porosity

The bulk density measured on discrete samples of serpentinized peridotites ranges 2.3–2.7 g/cm^3 (average = 2.55 ± 0.08 g/cm^3). The grain density ranges 2.5–2.7 g/cm^3 (average = 2.66 ± 0.05 g/cm^3). Bulk density and grain density increase slightly downhole. Bulk density in gabbros ranges 2.5–3.24 g/cm^3. The bulk density was measured downhole using the Hostile Environment Litho-Density Sonde during logging Run 1. The bulk density has a baseline value of ~2.6 g/cm^3, which best fits serpentinized peridotite. Inflections with higher bulk density values are indicative of gabbro.

The porosity of serpentinized peridotites ranges 1.7%–20.4% (average = 7.0% ± 3.7%). The porosity in gabbro has a range of 0.3%–to 13.6% (average = 3.7% ± 3.5%). Porosity in serpentinized peridotite and in gabbro is lower at shallower depths, higher between 200 and 300 mbsf, and then decreases with depth.

4.2.3.6.2. Sonic velocity

Sonic velocity on cube samples was measured along the three principal directions *x*, *y*, and *z* in the CRF. The average velocity of serpentinized ultramafic rocks is 4480 m/s and ranges 3442 m/s (serpentinized harzburgite; Section 399-U1601C-49R-4; 255.2 mbsf) to 5960 m/s (serpentinized dunite; Section 193R-1; 950.8 mbsf). The average velocity in gabbroic rocks is higher than that in serpentinized ultramafic rocks, 5906 m/s, ranging 4187 m/s (gabbronorite; Section 52R-2; 267.0 mbsf) to 6532 m/s (olivine gabbro; Section 32R-2; 170.3 mbsf). The apparent anisotropy of sonic velocity ranges 0.5% (gabbro; interval 22R-1, 56.5–58.5 cm; 120.6 mbsf) to 11.8% (serpentinized harzburgite; interval 148R-3, 113–115 cm; 734.9 mbsf). Sonic velocity was measured downhole using the Dipole Shear Sonic Imager (DSI) during logging Run 4. A baseline of *P*-wave velocity of ~4000 m/s and a baseline *S*-wave value of ~2000 m/s are reflective of the high proportion of serpentinized peridotites in Hole U1601C. Velocity overall increases with depth.

The Versatile Seismic Imager (VSI) was deployed during logging Run 5. A total of 13 stations spaced 100 m apart were measured in Hole U1601C. *P*-wave velocity measured using the VSI matches the velocities from the DSI. The average velocity across all stations is ~4500 m/s with a range of 3638 m/s at the shallowest depth (~58 mbsf) to 5299 m/s in the deepest part of the hole (~1070 mbsf). This is broadly comparable with existing seismic data.

4.2.3.6.3. Magnetic susceptibility

Magnetic susceptibility measured on the cores ranges 1,000–15,500 IU in serpentinized peridotite. Gabbro has magnetic susceptibility values that range 0–23,500 IU. The vast majority of gabbro have very low to zero magnetic susceptibility values (<100 IU). The main exceptions are Fe-Ti oxide gabbro that have the highest values of any rock type. Magnetic susceptibility was measured downhole with the Magnetic Susceptibility Sonde during logging Run 3. Magnetic susceptibility values are variable downhole, with the highest value matching the higher magnetic susceptibility measured in serpentinized peridotite cores. Downhole variations in magnetic susceptibility measured on cores and downhole match well.

4.2.3.6.4. Natural gamma radiation

NGR is low overall with both gabbros and serpentinized peridotites having values of <1 counts/s. The highest values of 3–13 counts/s occur in serpentinized peridotites. NGR was measured downhole using the Hostile Environment Natural Gamma Ray Sonde during logging Runs 1, 3, and 4. Downhole values are low below ~185 mbsf, with a baseline value of ~0.5 American Petroleum Institute gamma radiation units (gAPI). Between 30 mbsf (right below the logging bit) and ~185 mbsf, values are variable and as high as 35 gAPI. Standard spectral analysis by the commercial software yielded <0.1 wt% K, ~2 ppm U, and ~0.6 ppm Th, with some negative values indicating that the lower counts are below the threshold required to compute accurate K, U, and Th concentrations.

4.2.3.6.5. Electrical resistivity

Electrical resistivity was measured using the High-Resolution Laterolog Array tool during Run 2 and returned a baseline value of ~3.7 Ωm for the deep penetration. Gabbro is in general more resistive than serpentinized peridotite.

4.2.3.6.6. Borehole imaging

The Ultrasonic Borehole Imager was employed during logging Run 2, and the FMS was used during logging Run 4. The FMS logs are of good quality and cover the depth interval 72–1072 mbsf. Serpentinized peridotite has a mottled appearance, likely reflecting the different resistivities of phases present. Gabbro has a more consistent resistivity response. At least four distinct planar feature types can be identified including conductive planes (darker color, likely fractures), resistive planes (light color, likely veins), contacts (different textures), and fabrics.

4.2.3.6.7. Thermal conductivity

Thermal conductivity was measured on 48 archive section half samples selected from representative lithologies of Hole U1601C. A total of 38 ultramafic samples were measured, with thermal conductivity values ranging 2.20–3.56 W/(m·K) and a mean of 3.02 ± 0.26 W/(m·K). Ultramafic samples from Hole U1601C generally show higher thermal conductivity compared to those recovered from Hole U1601A (averaging 3.02 and 2.56 W/[m·K], respectively). A total of 20 gabbroic samples have generally lower thermal conductivity than the ultramafic samples, averaging 2.63 ± 0.54 W/(m·K), and contain much higher variability, ranging 2.04–4.09 W/(m·K).

4.2.3.6.8. Downhole temperature logging

Borehole fluid temperatures were measured several times in Hole U1601C. Five runs of the ETBS were conducted. Maximum temperatures recorded at the bottom of the borehole change over time, as fluids were warmed by the surrounding formation. Logging Run 1 reached 997.6 mbsf in the borehole ~17 h after flushing the hole with cool freshwater had ceased and recorded a maximum temperature of 70.3°C. Logging Run 4 measured a maximum temperature of 88.6°C at similar depths (1009 mbsf) ~64 h after flushing. Logging Run 5 recorded a maximum fluid temperature of 91.3°C at 1060 mbsf ~78 h after flushing.

4.2.3.7. Paleomagnetism

Remanence measurements were made on archive section halves from Holes U1601A and U1601C. These measurements generated 2,967 and 168,296 data points for Holes U1601A and U1601C demagnetization data sets, respectively, which helped determine the NRM of the rocks. Although the greater parts of the holes had NRM inclination values that generally clustered around an expected reversed geomagnetic polarity direction, the inclination values were quite variable. For Hole U1601A, the mean NRM inclination is −22.2° ± 13.5°, whereas for Hole U1601C the NRM inclination is −26.7° ± 32.8°. A low-coercivity drilling-induced component was removed by AF demagnetization steps of 10–15 mT, shifting the distribution closer to the expected GAD value of −49°. However, stronger AF steps (>40°) shift the inclination distribution toward the present-day polarity, which suggests that the rocks contain multiple component directions, thus capturing a complex remanence history. The timing of these remanence-affecting events (e.g., tectonic rotation and hydrothermal synthesis of magnetite) cannot be uniquely determined from these data and will require further synthesis of geologic data.

Archive section half data were complemented by discrete sample measurements. Both paleomagnetic and physical properties cube samples were analyzed using AF demagnetization, thermal demagnetization, IRM acquisition, and IRM backfield methods. Additionally, paleomagnetism cube samples were pretreated with liquid nitrogen dunking as a way of reducing the drilling overprint. Analysis of these data supported the variable nature in magnetic properties. The numerous high-quality discrete samples measured corroborate the variable inclination and intensity values of the archive section half data set. Although the bulk remanence of these rocks was carried by magnetite, some samples showed a significant magnetic contribution from gyroremanent minerals, likely some species of iron sulfide. Magnetite populations vary in terms of coercivity, likely indicating variable grain size and oxidation downhole for each hole.

AMS data were predominantly characterized by oblate magnetic fabrics. The relatively low recovery of Hole U1601A limited this type of analysis; thus, most of the AMS results were only meaningful for Hole U1601C. For Hole U1601C, the clustering of the shortest magnetic axis (K_{min}) around vertical indicates that the direction of magnetic flow was subhorizontal. Particular regions, however, display elongated fabrics, or regions of greater anisotropy. The regions of magnetic elongation correspond well with the depths of recovered deformed gabbro units (200 and 600 mbsf). These observations suggest that different interval depths experienced different tectonic and/or alteration histories.

5. Scientific assessment

5.1. Operations

Expedition 399 consisted of 46 operational days on station over the time frame from 12 April to 12 June 2023. By almost any measure, drilling operations during Expedition 399 were incredibly successful. Although we did not reach our preexpedition target depth of ~2060 mbsf in Hole U1309D, the lack of progress was entirely due to decisions by the Science Party to prioritize the continued successful drilling in Hole U1601C, where our scientific targets were far exceeded (Lissenberg et al., 2024). In doing so, we drilled the deepest hole ever initiated for a single oceanic hard rock scientific expedition, previously accomplished during IODP Expedition 360 in Hole U1473A (789.7 mbsf) (Tables **T1**, **T2**). Previous holes drilled to >1000 mbsf required 12–98 bit runs over 2–8 expeditions (Table **T2**) to reach the full depth. In comparison, Hole U1601C was drilled with only 8 total bit runs (5 coring runs) and had remarkable core recoveries over the entire hole averaging 71%, with 24% of cores achieving recoveries >90%. Access to a continuous record through extended sections of the hole will provide robust constraints on the architecture and composition of the oceanic mantle lithosphere.

Three water sampling campaigns recovered high-quality borehole fluids from both Holes U1601C and U1309D, including the inaugural deployment of the MTFS, which provided larger volumes at each depth and was designed for chemical compatibility for geochemical species of interest. The success rate of water sampler deployments was overall ~50% for the MTFS and 70% for the KFTS, which compares well to previous expeditions in Hole 504B and at Brothers Volcano (de Ronde et al., 2019).

A full suite of logging operations carried out in Hole U1601C obtained high-quality data to complement and extend the data from recovered cores. The thermal profile of the hole was documented as it rebounded after extensive flushing, while magnetic susceptibility will provide further constraints on the distributions of gabbro and serpentinized peridotite downhole. Image logs can be used to reorient contacts of collected cores.

Significant challenges were encountered during shipboard processing of cores. The high recovery and rapid drilling rates imposed a significant strain on the technical staff and Science Party whose numbers were already limited because of Coronavirus Disease 2019 (COVID-19) restrictions and the absence of two members for last-minute personal reasons. From 6 to 22 May 22, 5 m core intervals with almost complete recoveries were recovered every 1 h and 45 min with only a few longer breaks during bit changes. Coring rates eventually slowed when intervals dominated by gabbroic lithologies were encountered.

The recognition of chrysotile in hydrothermally altered peridotite cores triggered a halt of many core processing activities. For full details see **Operations** in the Expedition 399 methods chapter (Lang et al., 2025a) and McCaig et al. (2024)

5.2. Scientific objectives

5.2.1. Objective 1: characterizing the life cycle of an oceanic core complex and the links among igneous, metamorphic, structural, and fluid flow processes

Hole U1601C is a unique 1268 m section through serpentinized mantle rocks containing numerous gabbroic (lower crustal) intrusions. When combined with Hole U1309D (deepened to 1498 mbsf during Expedition 399), the shallow holes of Expedition 357, and seismic data (Figure **F1**), we have by far the most comprehensive data set on the life cycle of a typical mafic/ultramafic OCC (Lissenberg et al., 2024).

The life cycle of a core complex begins with mantle rocks uplifted by corner flow in the spreading environment and affected by high-temperature partial melting and porous flow of melts. These processes are evident through observations of dunite veins and the growth of secondary orthopyroxene in harzburgite. The products of partial melting at deeper levels are also seen intruded as a complex network of more than 400 gabbroic intrusions in the section cored in Hole U1601C. Melt-rock reaction textures are also seen in the gabbroic pluton sampled in Hole U1309D, indicating the complexity of the melting and intrusion processes in the Atlantic Massif.

Further unroofing at subsolidus temperatures was accommodated by deformation and hydrothermal alteration over waning temperature conditions. Strain accommodated by crystal-plastic deformation at temperatures >600°C was overprinted by brittle faulting, cataclasis, and hydrothermal veining at Site U1601, recording a new cataclastic fault zone in Hole U1309D. Hydrothermal fluids infiltrated the rocks, probably in small quantities, at temperatures >700°C. Further hydration reactions occurred in amphibolite and greenschist facies in gabbroic rocks, particularly close to contacts with ultramafic rocks. High fluid fluxes in some zones are indicated by intense alteration, including dissolution of minerals to form macroscopic reaction porosity. The most ubiquitous alteration is serpentinization of peridotite, likely occurring at 200°–350°C (Klein et al., 2014), probably before complete unroofing of the massif by detachment faulting.

The latest phase in the life cycle of the Atlantis Massif is uplift of the unroofed massif, hydrothermal circulation forming the LCHF, and low-temperature alteration and subseafloor weathering. Hole U1601C is ideal for investigating the hydrogeology and thermal structure of the massif, and preliminary temperature results from logging indicate borehole fluid temperatures >90°C at 1060 mbsf. Because of vigorous fluid circulation at the end of drilling, this is a minimum temperature for the surrounding rock, and metamorphic reactions could be occurring at ambient temperatures well over 100°C in the rocks surrounding the borehole.

5.2.2. Objective 2: accessing the chemical kitchen that preceded the appearance of life on Earth

A major goal of the expedition was to link abundances of H_2 and organic molecules with the physical and chemical conditions that lead to their synthesis. Of particular interest was accessing zones where active serpentinization could lead to the production of H_2 and zones above the temperature limit of life to examine geochemical reactions without a biological overprint.

In Hole U1309D we successfully recovered cores and fluids from zones at temperatures of 140°C, well above the currently recognized limit to life. Olivine gabbro and olivine-bearing gabbro were abundant, and in some cases, olivine was replaced by secondary minerals including serpentine, magnetite, and clay, which can be associated with H_2 production and organic carbon formation. Fluid inclusions in olivine, possibly containing H_2 and/or CH_4, were locally abundant. The geochemistry of the sampled fluids indicates they were a mix of seawater, formation water, and reacted water from the base of the hole.

Site U1601 was primarily chosen to access an actively serpentinizing environment. The dominant lithology in Holes U1601A and U1601C is harzburgite that has been variably altered to magnetite-bearing serpentinite, suggestive of H_2 formation and reducing conditions. Fluid inclusions, possibly containing H_2 and/or CH_4, were abundant in many of the thin sections that could be examined from Site U1601. The achieved drilling depths may have accessed a thermal regime above the limit of life because downhole temperature logs recorded a maximum of 91°C within 78 h of flushing with shipboard freshwater, prior to full equilibration of fluids. Elevated concentrations of hydrogen and methane were detected in fluids recovered by the borehole samplers, suggesting serpentinization is active and ongoing or that pockets of volatile-rich fluids were liberated during drilling. The relationship of volatile distributions with depth, temperature, lithology, and other processes will provide insights into the processes that lead to their formation.

Shore-based analyses will greatly advance this objective. Fluids and rocks will be analyzed for the concentrations and isotopes of organic compounds to identify the forms of reduced carbon present in the subseafloor. Fluid inclusions have been identified in the few peridotite, olivine-gabbro, and troctolite thin sections that were available shipboard; further sampling and analysis will be needed to determine the extent of their distributions and the content of the inclusions. Similarly, shore-based analyses such as Fe-titrations will provide quantitative constraints on the valence of Fe and the formation of H_2.

A second major goal was to leave both the deepened Hole U1309D and the new peridotite-hosted hole at Site U1601 in a condition such that future expeditions could relog them for temperature and conduct fluid sampling. Prior to our departure, both holes were flushed with seven borehole volumes of seawater to expel drill cuttings and other debris. To the best of our knowledge, no significant material related to drilling or logging operations was left in the holes, and the camera surveys at the exit of the last bit runs indicated that the reentry cones remained intact.

5.2.3. Objective 3: characterizing the deep biosphere and limits for life in the Atlantis Massif, in particular the impact of lithospheric substrate, porosity, permeability, temperature, fluid chemistry, and reactive gradients

Rocks and fluids were extensively sampled to assess the extent of the deep biosphere and limits of life in Holes U1309D, U1601A, and U1601C. The depth of Hole U1601C provides an opportunity to sample material from near subseafloor zones that appear to be more extensively weathered by interaction with oxic seawater, warm anoxic zones in which hydrothermal alteration is extensive and serpentinization appears to be ongoing, and a deep regime that may be at temperatures above the limits of life.

A target for the expedition was to preferentially sample zones of higher porosity and permeability to test whether these regimes are associated with greater microbial biomass and activity. Samples were selected for microbiological analysis in collaboration with a petrologist representing the core description teams so that low(er) temperature alteration phases could be preferentially sampled. Geochemical analyses indicate that the microbiology samples were more carbonate rich than average background samples.

The microbiology samples were extensively documented with general descriptions, 360° imaging, and geochemical analyses including shipboard inductively coupled plasma–atomic emission spectroscopy and coulometry. Because of the absence of other samples available for many shipboard measurements, the exteriors of microbiology samples were also subjected to more extensive analyses than is typically performed, such as porosity and density. The combined data set will allow robust insights into the physical and geochemical properties of locations where higher cellular abundances and indications of active metabolism are identified by shore-based analyses.

References

Allen, D.E., and Seyfried, W.E., 2004. Serpentinization and heat generation: constraints from Lost City and Rainbow hydrothermal systems. Geochimica et Cosmochimica Acta, 68(6):1347–1354. **https://doi.org/10.1016/j.gca.2003.09.003**

Allen, D.E., and Seyfried, W.E., 2005. REE controls in ultramafic hosted MOR hydrothermal systems: an experimental study at elevated temperature and pressure. Geochimica et Cosmochimica Acta, 69(3):675–683. **https://doi.org/10.1016/j.gca.2004.07.016**

Andreani, M., Montagnac, G., Fellah, C., Hao, J., Vandier, F., Daniel, I., Pisapia, C., Galipaud, J., Lilley, M.D., Früh Green, G.L., Borensztajn, S., and Ménez, B., 2023. The rocky road to organics needs drying. Nature Communications, 14(1):347. **https://doi.org/10.1038/s41467-023-36038-6**

Andreani, M., Muñoz, M., Marcaillou, C., and Delacour, A., 2013. µXANES study of iron redox state in serpentine during oceanic serpentinization. Lithos, 178:70–83. **https://doi.org/10.1016/j.lithos.2013.04.008**

Beard, J.S., Frost, B.R., Fryer, P., McCaig, A., Searle, R., Ildefonse, B., Zinin, P., and Sharma, S.K., 2009. Onset and progression of serpentinization and magnetite formation in olivine-rich troctolite from IODP Hole U1309D. Journal of Petrology, 50(3):387–403. **https://doi.org/10.1093/petrology/egp004**

Becker, K., Davis, E.E., Spiess, F.N., and deMoustier, C.P., 2004. Temperature and video logs from the upper oceanic crust, Holes 504B and 896A, Costa Rica Rift flank; implications for the permeability of upper oceanic crust. Earth and Planetary Science Letters, 222(3–4):881–896. **https://doi.org/10.1016/j.epsl.2004.03.033**

Blackman, D., Slagle, A., Harding, A., Guerin, G., and McCaig, A., 2013. IODP Expedition 340T: borehole logging at Atlantis Massif oceanic core complex. Scientific Drilling, 15:31–35. **https://doi.org/10.2204/iodp.sd.15.04.2013**

Blackman, D.K., Cann, J.R., Janssen, B., and Smith, D.K., 1998. Origin of extensional core complexes: evidence from the Mid-Atlantic Ridge at Atlantis Fracture Zone. Journal of Geophysical Research: Solid Earth, 103(B9):21315–21333. **https://doi.org/10.1029/98JB01756**

Blackman, D.K., Ildefonse, B., John, B.E., MacLeod, C.J., Ohara, Y., Miller, D.J., and the Expedition 304/305 Project Team, 2004. Oceanic core complex formation, Atlantis Massif—oceanic core complex formation, Atlantis Massif, Mid-Atlantic Ridge: drilling into the footwall and hanging wall of a tectonic exposure of deep, young oceanic lithosphere to study deformation, alteration, and melt generation. Integrated Ocean Drilling Program Scientific Prospectus, 304/305. **https://doi.org/10.2204/iodp.sp.304305.2004**

Blackman, D.K., Ildefonse, B., John, B.E., Ohara, Y., Miller, D.J., Abe, N., Abratis, M., Andal, E.S., Andreani, M., Awaji, S., Beard, J.S., Brunelli, D., Charney, A.B., Christie, D.M., Collins, J., Delacour, A.G., Delius, H., Drouin, M., Einaudi, F., Escartin, J., Frost, B.R., Früh-Green, G., Fryer, P.B., Gee, J.S., Godard, M., Grimes, C.B., Halfpenny, A., Hansen, H.E., Harris, A.C., Tamura, A., Hayman, N.W., Hellebrand, E., Hirose, T., Hirth, J.G., Ishimaru, S., Johnson, K.T.M., Karner, G.D., Linek, M., MacLeod, C.J., Maeda, J., Mason, O.U., McCaig, A.M., Michibayashi, K., Morris, A., Nakagawa, T., Nozaka, T., Rosner, M., Searle, R.C., Suhr, G., Tominaga, M., von der Handt, A., Yamasaki, T., and Zhao, X., 2011. Drilling constraints on lithospheric accretion and evolution at Atlantis Massif, Mid-Atlantic Ridge 30°N. Journal of Geophysical Research: Solid Earth, 116(B7):B07103. **https://doi.org/10.1029/2010JB007931**

Blackman, D.K., Ildefonse, B., John, B.E., Ohara, Y., Miller, D.J., MacLeod, C.J., and the Expedition 304/305 Scientists, 2006. Proceedings of the Integrated Ocean Drilling Program, 304/305: College Station, TX (Integrated Ocean Drilling Program Management International, Inc.). **https://doi.org/10.2204/iodp.proc.304305.2006**

Blackman, D.K., Karson, J.A., Kelley, D.S., Cann, J.R., Früh-Green, G.L., Gee, J.S., Hurst, S.D., John, B.E., Morgan, J., Nooner, S.L., Ross, D.K., Schroeder, T.J., and Williams, E.A., 2002. Geology of the Atlantis Massif (Mid-Atlantic Ridge, 30°N): Implications for the evolution of an ultramafic oceanic core complex. Marine Geophysical Research, 23(5):443–469. **https://doi.org/10.1023/B:MARI.0000018232.14085.75**

Blackman, D.K., Slagle, A.L., Guerin, G., and Harding, A., 2014. Geophysical signatures of past and present hydration within a young oceanic core complex. Geophysical Research Letters, 41(4):1179–1186. **https://doi.org/10.1002/2013GL058111**

Boschi, C., Früh-Green, G.L., Delacour, A., Karson, J.A., and Kelley, D.S., 2006. Mass transfer and fluid flow during detachment faulting and development of an oceanic core complex, Atlantis Massif (MAR 30°N). Geochemistry, Geophysics, Geosystems, 7(1):Q01004. **https://doi.org/10.1029/2005GC001074**

Bradley, A.S., Hayes, J.M., and Summons, R.E., 2009. Extraordinary ^{13}C enrichment of diether lipids at the Lost City hydrothermal field indicates a carbon-limited ecosystem. Geochimica et Cosmochimica Acta, 73(1):102–118. **https://doi.org/10.1016/j.gca.2008.10.005**

Brazelton, W.J., and Baross, J.A., 2010. Metagenomic comparison of two Thiomicrospira lineages inhabiting contrasting deep-sea hydrothermal environments. PLOS ONE, 5(10):e13530. **https://doi.org/10.1371/journal.pone.0013530**

Brazelton, W.J., Ludwig, K.A., Sogin, M.L., Andreishcheva, E.N., Kelley, D.S., Shen, C.-C., Edwards, R.L., and Baross, J.A., 2010. Archaea and bacteria with surprising microdiversity show shifts in dominance over 1,000-year time scales in hydrothermal chimneys. Proceedings of the National Academy of Sciences of the United States of America, 107(4):1612–1617. **https://doi.org/10.1073/pnas.0905369107**

Brazelton, W.J., Schrenk, M.O., Kelley, D.S., and Baross, J.A., 2006. Methane- and sulfur-metabolizing microbial communities dominate the Lost City hydrothermal field ecosystem. Applied and Environmental Microbiology, 72(9):6257–6270. **https://doi.org/10.1128/AEM.00574-06**

Canales, J.P., Tucholke, B.E., and Collins, J.A., 2004. Seismic reflection imaging of an oceanic detachment fault: Atlantis megamullion (Mid-Atlantic Ridge, 30°10′N). Earth and Planetary Science Letters, 222(2):543–560. **https://doi.org/10.1016/j.epsl.2004.02.023**

Canales, J.P., Tucholke, B.E., Xu, M., Collins, J.A., and DuBois, D.L., 2008. Seismic evidence for large-scale compositional heterogeneity of oceanic core complexes. Geochemistry, Geophysics, Geosystems, 9(8):Q08002. **https://doi.org/10.1029/2008GC002009**

Cann, J.R., Blackman, D.K., Smith, D.K., McAllister, E., Janssen, B., Mello, S., Avgerinos, E., Pascoe, A.R., and Escartin, J., 1997. Corrugated slip surfaces formed at ridge–transform intersections on the Mid-Atlantic Ridge. Nature, 385(6614):329–332. **https://doi.org/10.1038/385329a0**

Cann, J.R., McCaig, A.M., and Yardley, B.W.D., 2015. Rapid generation of reaction permeability in the roots of black smoker systems, Troodos ophiolite, Cyprus. Geofluids, 15(1–2):179–192. **https://doi.org/10.1111/gfl.12117**

Cannat, M., 1996. How thick is the magmatic crust at slow spreading oceanic ridges? Journal of Geophysical Research: Solid Earth, 101(B2):2847–2857. **https://doi.org/10.1029/95JB03116**

Cannat, M., Karson, J.A., Miller, D.J., et al., 1995. Proceedings of the Ocean Drilling Program, Initial Reports, 153: College Station, TX (Ocean Drilling Program). **https://doi.org/10.2973/odp.proc.ir.153.1995**

Coogan, L.A., Kempton, P.D., Saunders, A.D., and Norry, M.J., 2000a. Melt aggregation within the crust beneath the Mid-Atlantic Ridge: evidence from plagioclase and clinopyroxene major and trace element compositions. Earth and Planetary Science Letters, 176(2):245–257. **https://doi.org/10.1016/S0012-821X(00)00006-6**

Coogan, L.A., Saunders, A.D., Kempton, P.D., and Norry, M.J., 2000b. Evidence from oceanic gabbros for porous melt migration within a crystal mush beneath the Mid-Atlantic Ridge. Geochemistry, Geophysics, Geosystems, 1(9). **https://doi.org/10.1029/2000GC000072**

Cotterill, C., and Früh-Green, G.L., 2021. Multibeam bathymetry processed data (Kongsberg EM 122 working area dataset) of RRS JAMES COOK during cruise IODP Expedition 357, Atlantis Massif. **https://doi.org/10.1594/PANGAEA.935687**

de Ronde, C.E.J., Humphris, S.E., Höfig, T.W., Brandl, P.A., Cai, L., Cai, Y., Caratori Tontini, F., Deans, J.R., Farough, A., Jamieson, J.W., Kolandaivelu, K.P., Kutovaya, A., Labonté, J.M., Martin, A.J., Massiot, C., McDermott, J.M., McIntosh, I.M., Nozaki, T., Pellizari, V.H., Reyes, A.G., Roberts, S., Rouxel, O., Schlicht, L.E.M., Seo, J.H., Straub, S.M., Strehlow, K., Takai, K., Tanner, D., Tepley III, F.J., and Zhang, C., 2019. Expedition 376 methods. In de Ronde, C.E.J., Humphris, S.E., Höfig, T.W., and the Expedition 376 Scientists, Brothers Arc Flux. Proceedings of the International Ocean Discovery Program, 376: College Station, TX (International Ocean Discovery Program). **https://doi.org/10.14379/iodp.proc.376.102.2019**

Denny, A.R., Kelley, D.S., and Früh-Green, G.L., 2016. Geologic evolution of the Lost City Hydrothermal Field. Geochemistry, Geophysics, Geosystems, 17(2):375–394. **https://doi.org/10.1002/2015GC005869**

Detrick, R.S., and Collins, J.A., 1998. Seismic structure of ultramafics exposed at shallow crustal levels in the Mid-Atlantic Ridge rift valley at 15°N. Eos, Transactions of the American Geophysical Union, 79:F800.

Dick, H.J.B., MacLeod, C.J., Blum, P., Abe, N., Blackman, D.K., Bowles, J.A., Cheadle, M.J., Cho, K., Ciazela, J., Deans, J.R., Edgcomb, V.P., Ferrando, C., France, L., Ghosh, B., Ildefonse, B.M., Kendrick, M.A., Koepke, J.H., Leong, J.A.M., Chuanzhou, L., Qiang, M., Morishita, T., Morris, A., Natland, J.H., Nozaka, T., Pluemper, O., Sanfilippo, A., Sylvan, J.B., Tivey, M.A., Tribuzio, R., and Viegas, L.G.F., 2017. Expedition 360 summary. In MacLeod, C.J., Dick, H.J.B., Blum, P., and the Expedition 360 Scientists, Southwest Indian Ridge Lower Crust and Moho. Proceedings of the International Ocean Discovery Program, 360: College Station, TX (International Ocean Discovery Program). **https://doi.org/10.14379/iodp.proc.360.101.2017**

Drouin, M., Godard, M., Ildefonse, B., Bruguier, O., and Garrido, C.J., 2009. Geochemical and petrographic evidence for magmatic impregnation in the oceanic lithosphere at Atlantis Massif, Mid-Atlantic Ridge (IODP Hole U1309D, 30°N). Chemical Geology, 264(1):71–88. **https://doi.org/10.1016/j.chemgeo.2009.02.013**

Drouin, M., Ildefonse, B., and Godard, M., 2010. A microstructural imprint of melt impregnation in slow spreading lithosphere: olivine-rich troctolites from the Atlantis Massif, Mid-Atlantic Ridge, 30°N, IODP Hole U1309D. Geochemistry, Geophysics, Geosystems, 11(6):Q06003. **https://doi.org/10.1029/2009GC002995**

Escartín, J., and Canales, J.P., 2011. Detachments in oeanic lithosphere: deformation, magmatism, fluid flow, and ecosystems. Eos, Transactions American Geophysical Union, 92(4):31. **https://doi.org/10.1029/2011EO040003**

Escartín, J., John, B., Cannat, M., Olive, J.-A., Cheadle, M., Früh-Green, G., and Cotterill, C., 2022. Tectonic termination of oceanic detachment faults, with constraints on tectonic uplift and mass wasting related erosion rates. Earth and Planetary Science Letters, 584:117449. **https://doi.org/10.1016/j.epsl.2022.117449**

Expedition 340T Scientists, 2012. Atlantis Massif Oceanic Core Complex: velocity, porosity, and impedance contrasts within the domal core of Atlantis Massif: faults and hydration of lithosphere during core complex evolution. Integrated Ocean Drilling Program Preliminary Report, 340T. **https://doi.org/10.2204/iodp.pr.340T.2012**

Ferrando, C., Godard, M., Ildefonse, B., and Rampone, E., 2018. Melt transport and mantle assimilation at Atlantis Massif (IODP Site U1309): constraints from geochemical modeling. Lithos, 323:24–43. **https://doi.org/10.1016/j.lithos.2018.01.012**

Ferrando, C., Lynn, K.J., Basch, V., Ildefonse, B., and Godard, M., 2020. Retrieving timescales of oceanic crustal evolution at oceanic core complexes: insights from diffusion modelling of geochemical profiles in olivine. Lithos, 376–377:105727. **https://doi.org/10.1016/j.lithos.2020.105727**

Foustoukos, D.I., Savov, I.P., and Janecky, D.R., 2008. Chemical and isotopic constraints on water/rock interactions at the Lost City hydrothermal field, 30°N Mid-Atlantic Ridge. Geochimica et Cosmochimica Acta, 72(22):5457–5474. **https://doi.org/10.1016/j.gca.2008.07.035**

Foustoukos, D.I., and Seyfried, W.E., 2004. Hydrocarbons in hydrothermal vent fluids: the role of chromium-bearing catalysts. Science, 304(5673):1002–1005. **https://doi.org/10.1126/science.1096033**

Frost, B.R., Beard, J.S., McCaig, A., and Condliffe, E., 2008. The formation of micro-rodingites from IODP Hole U1309D: key to understanding the process of serpentinization. Journal of Petrology, 49(9):1579–1588. **https://doi.org/10.1093/petrology/egn038**

Früh-Green, G.L., Kelley, D.S., Bernasconi, S.M., Karson, J.A., Ludwig, K.A., Butterfield, D.A., Boschi, C., and Proskurowski, G., 2003. 30,000 years of hydrothermal activity at the Lost City vent field. Science, 301(5632):495–498. **https://doi.org/10.1126/science.1085582**

Früh-Green, G.L., Orcutt, B.N., Green, S., Cotterill, C., and the Expedition 357 Scientists, 2016. Expedition 357 Preliminary Report: Atlantis Massif Serpentinization and Life. International Ocean Discovery Program. **https://doi.org/10.14379/iodp.pr.357.2016**

Früh-Green, G.L., Orcutt, B.N., Green, S.L., Cotterill, C., Morgan, S., Akizawa, N., Bayrakci, G., Behrmann, J.-H., Boschi, C., Brazelton, W.J., Cannat, M., Dunkel, K.G., Escartin, J., Harris, M., Herrero-Bervera, E., Hesse, K., John, B.E., Lang, S.Q., Lilley, M.D., Liu, H.-Q., Mayhew, L.E., McCaig, A.M., Menez, B., Morono, Y., Quéméneur, M., Rouméjon, S., Sandaruwan Ratnayake, A., Schrenk, M.O., Schwarzenbach, E.M., Twing, K.I., Weis, D., Whattam, S.A., Williams, M., and Zhao, R., 2017. Expedition 357 summary. In Früh-Green, G.L., Orcutt, B.N., Green, S.L., Cotterill, C., and the Expedition 357 Scientists, Atlantis Massif Serpentinization and Life. Proceedings of the International Ocean Discovery Program, 357: College Station, TX (International Ocean Discovery Program). **https://doi.org/10.14379/iodp.proc.357.101.2017**

Früh-Green, G.L., Orcutt, B.N., Rouméjon, S., Lilley, M.D., Morono, Y., Cotterill, C., Green, S., Escartin, J., John, B.E., McCaig, A.M., Cannat, M., Ménez, B., Schwarzenbach, E.M., Williams, M.J., Morgan, S., Lang, S.Q., Schrenk, M.O., Brazelton, W.J., Akizawa, N., Boschi, C., Dunkel, K.G., Quéméneur, M., Whattam, S.A., Mayhew, L., Harris, M., Bayrakci, G., Behrmann, J.-H., Herrero-Bervera, E., Hesse, K., Liu, H.-Q., Ratnayake, A.S., Twing, K., Weis, D., Zhao, R., and Bilenker, L., 2018. Magmatism, serpentinization and life: insights through drilling the Atlantis Massif (IODP Expedition 357). Lithos, 323:137–155. **https://doi.org/10.1016/j.lithos.2018.09.012**

Gillis, K., Mével, C, Allan, J., et al., 1993. Proceedings of the Ocean Drilling Program, Initial Reports, 147: College Station, TX (Ocean Drilling Program). **https://doi.org/10.2973/odp.proc.ir.147.1993**

Gillis, K.M., Snow, J.E., Klaus, A., Guerin, G., Abe, N., Akizawa, N., Ceuleneer, G., Cheadle, M.J., Adrião, Á., Faak, K., Falloon, T.J., Friedman, S.A., Godard, M.M., Harigane, Y., Horst, A.J., Hoshide, T., Ildefonse, B., Jean, M.M., John, B.E., Koepke, J.H., Machi, S., Maeda, J., Marks, N.E., McCaig, A.M., Meyer, R., Morris, A., Nozaka, T., Python, M., Saha, A., and Wintsch, R.P., 2014. Expediton 345 summary. In Gillis, K.M., Snow, J.E., Klaus, A., and the Expedition 345 Scientists, Proceedings of the Integrated Ocean Drilling Program. 345: College Station, TX (Integrated Ocean Drilling Program). **https://doi.org/10.2204/iodp.proc.345.101.2014**

Godard, M., Awaji, S., Hansen, H., Hellebrand, E., Brunelli, D., Johnson, K., Yamasaki, T., Maeda, J., Abratis, M., Christie, D., Kato, Y., Mariet, C., and Rosner, M., 2009. Geochemistry of a long in-situ section of intrusive slow-spread oceanic lithosphere: results from IODP Site U1309 (Atlantis Massif, 30°N Mid-Atlantic-Ridge). Earth and Planetary Science Letters, 279(1–2):110–122. **https://doi.org/10.1016/j.epsl.2008.12.034**

Godard, M., Lagabrielle, Y., Alard, O., and Harvey, J., 2008. Geochemistry of the highly depleted peridotites drilled at ODP Sites 1272 and 1274 (Fifteen-Twenty Fracture Zone, Mid-Atlantic Ridge): implications for mantle dynamics beneath a slow spreading ridge. Earth and Planetary Science Letters, 267(3):410–425. **https://doi.org/10.1016/j.epsl.2007.11.058**

Goordial, J., D'Angelo, T., Labonté, J.M., Poulton, N.J., Brown, J.M., Stepanauskas, R., Früh-Green, G.L., Orcutt, B.N., and Dubilier, N., 2021. Microbial diversity and function in shallow subsurface sediment and oceanic lithosphere of the Atlantis Massif. mBio, 12(4):e00490-00421. **https://journals.asm.org/doi/abs/10.1128/mBio.00490-21**

Grimes, C.B., John, B.E., Cheadle, M.J., and Wooden, J.L., 2008. Protracted construction of gabbroic crust at a slow spreading ridge; constraints from $^{206}Pb/^{238}U$ zircon ages from Atlantis Massif and IODP Hole U1309D (30°N, MAR). Geochemistry, Geophysics, Geosystems, 9(8):Q08012. **https://doi.org/10.1029/2008GC002063**

Harding, A.J., Arnulf, A.F., and Blackman, D.K., 2016. Velocity structure near IODP Hole U1309D, Atlantis Massif, from waveform inversion of streamer data and borehole measurements. Geochemistry, Geophysics, Geosystems, 17(6):1990–2014. **https://doi.org/10.1002/2016GC006312**

Henig, A.S., Blackman, D.K., Harding, A.J., Canales, J.-P., and Kent, G.M., 2012. Downward continued multichannel seismic refraction analysis of Atlantis Massif oceanic core complex, 30°N, Mid-Atlantic Ridge. Geochemistry, Geophysics, Geosystems, 13(5):Q0AG07. **https://doi.org/10.1029/2012GC004059**

Heuer, V.B., Inagaki, F., Morono, Y., Kubo, Y., Spivack, A.J., Viehweger, B., Treude, T., Beulig, F., Schubotz, F., Tonai, S., Bowden, S.A., Cramm, M., Henkel, S., Hirose, T., Homola, K., Hoshino, T., Ijiri, A., Imachi, H., Kamiya, N., Kaneko, M., Lagostina, L., Manners, H., McClelland, H.-L., Metcalfe, K., Okutsu, N., Pan, D., Raudsepp, M.J., Sauvage, J., Tsang, M.-Y., Wang, D.T., Whitaker, E., Yamamoto, Y., Yang, K., Maeda, L., Adhikari, R.R., Glombitza, C., Hamada, Y., Kallmeyer, J., Wendt, J., Wörmer, L., Yamada, Y., Kinoshita, M., and Hinrichs, K.-U., 2020. Temperature limits to deep subseafloor life in the Nankai Trough subduction zone. Science, 370(6521):1230–1234. **https://doi.org/10.1126/science.abd7934**

Ildefonse, B., Abe, N., Godard, M., Morris, A., Teagle, D.A.H., and Umino, S., 2014. Formation and evolution of oceanic lithosphere: new insights on crustal structure and igneous geochemistry from ODP/IODP Sites 1256, U1309, and U1415. In Stein, R., Blackman, D.K., Inagaki, F., and Larsen, H.-C. (Eds.), Earth and Life Processes Discovered from Subseafloor Environments: A Decade of Science Achieved by the Integrated Ocean Drilling Program (IODP). R. Stein (Series Ed.). Developments in Marine Geology, 7: New York (Elsevier), 449–505. **https://doi.org/10.1016/B978-0-444-62617-2.00017-7**

Ildefonse, B., Blackman, D., John, B.E., Ohara, Y., Miller, D.J., MacLeod, C., and the Integrated Ocean Drilling Program Expeditions 304/305 Science Party, 2007. Oceanic core complexes and crustal accretion at slow-spreading ridges. Geology, 35(7):623–626. **https://doi.org/10.1130/G23531A.1**

John, B.E., Cheadle, M.J., Gee, J.S., Grimes, C.B., Morris, A., and Pressling, N., 2009. Data report: spatial and temporal evolution of slow spread oceanic crust; graphic sections of core recovered from IODP Hole U1309D, Atlantis Massif, 30°N, MAR (including Pb/U zircon geochronology and magnetic remanence data). In Blackman, D.K., Ildefonse, B., John, B.E., Ohara, Y., Miller, D.J., MacLeod, C.J., and the Expedition 304/305 Scientists, Proceedings of the Integrated Ocean Drilling Program. 304/305: College Station, TX (Integrated Ocean Drilling Program Management International, Inc.). **https://doi.org/10.2204/iodp.proc.304305.205.2009**

Kallmeyer, J., 2017. Contamination control for scientific drilling operations. In Sariaslani, S. and Gadd, G.M., Advances in Applied Microbiology (Volume 98). Cambridge, MA (Academic Press), 61–91. **https://doi.org/10.1016/bs.aambs.2016.09.003**

Karson, J.A., Cannat, M., Miller, J., and the ODP Leg 153 Shipboard Scientific Party, 1997. Drilling tectonic windows into the lower crust and upper mantle: ODP Leg 153. JOIDES Journal, 23(1):14–15. **http://www-odp.tamu.edu/publications/citations/joides_j/joides_j_23_1.pdf#page=14**

Karson, J.A., Früh-Green, G.L., Kelley, D.S., Williams, E.A., Yoerger, D.R., and Jakuba, M., 2006. Detachment shear zone of the Atlantis Massif core complex, Mid-Atlantic Ridge, 30°N. Geochemistry, Geophysics, Geosystems, 7(6):Q06016. **https://doi.org/10.1029/2005GC001109**

Kelemen, P.B., Kikawa, E., Miller, D.J., et al., 2004. Proceedings of the Ocean Drilling Program, Initial Reports, 209: College Station, TX (Ocean Drilling Program). **https://doi.org/10.2973/odp.proc.ir.209.2004**

Kelley, D.S., Baross, J.A., and Delaney, J.R., 2002a. Volcanoes, fluids, and life at mid-ocean ridge spreading centers. Annual Review of Earth and Planetary Sciences, 30(1):385–491. **https://doi.org/10.1146/annurev.earth.30.091201.141331**

Kelley, D.S., and Früh-Green, G.L., 1999. Abiogenic methane in deep-seated mid-ocean ridge environments: Insights from stable isotope analyses. Journal of Geophysical Research: Solid Earth, 104(B5):10439–10460. **https://doi.org/10.1029/1999JB900058**

Kelley, D.S., and Früh-Green, G.L., 2001. Volatile lines of descent in submarine plutonic environments: insights from stable isotope and fluid inclusion analyses. Geochimica et Cosmochimica Acta, 65(19):3325–3346. **https://doi.org/10.1016/S0016-7037(01)00667-6**

Kelley, D.S., Karson, J.A., Blackman, D.K., Früh-Green, G.L., Butterfield, D.A., Lilley, M.D., Olson, E.J., Schrenk, M.O., Roe, K.K., Lebon, G.T., Rivizzigno, P., and the AT3-60 Shipboard Party, 2001. An off-axis hydrothermal vent field near the Mid-Atlantic Ridge at 30°N. Nature, 412(6843):145–149. **https://doi.org/10.1038/35084000**

Kelley, D.S., Karson, J.A., Früh-Green, G., and Schrenk, M.O., 2002b. Ultramafic-hosted hydrothermal systems: the Lost City Field as a possible guide for early life. Astrobiology, 2(4):449–450.

Kelley, D.S., Karson, J.A., Früh-Green, G.L., Yoerger, D.R., Shank, T.M., Butterfield, D.A., Hayes, J.M., Schrenk, M.O., Olson, E.J., Proskurowski, G., Jakuba, M., Bradley, A., Larson, B., Ludwig, K., Glickson, D., Buckman, K., Bradley, A.S., Brazelton, W.J., Roe, K., Elend, M.J., Delacour, A.l., Bernasconi, S.M., Lilley, M.D., Baross, J.A., Summons, R.E., and Sylva, S.P., 2005. A serpentinite-hosted ecosystem: the Lost City hydrothermal field. Science, 307(5714):1428–1434. **https://doi.org/10.1126/science.1102556**

Klein, F., Bach, W., Humphris, S.E., Kahl, W.-A., Jöns, N., Moskowitz, B., and Berquó, T.S., 2014. Magnetite in seafloor serpentinite—Some like it hot. Geology, 42(2):135–138. **https://doi.org/10.1130/G35068.1**

Klein, F., Bach, W., Jöns, N., McCollom, T., Moskowitz, B., and Berquó, T., 2009. Iron partitioning and hydrogen generation during serpentinization of abyssal peridotites from 15°N on the Mid-Atlantic Ridge. Geochimica et Cosmochimica Acta, 73(22):6868–6893. **https://doi.org/10.1016/j.gca.2009.08.021**

Klein, F., Bach, W., and McCollom, T.M., 2013. Compositional controls on hydrogen generation during serpentinization of ultramafic rocks. Lithos, 178:55–69. **https://doi.org/10.1016/j.lithos.2013.03.008**

Klein, F., Grozeva, N.G., and Seewald, J.S., 2019. Abiotic methane synthesis and serpentinization in olivine-hosted fluid inclusions. Proceedings of the National Academy of Sciences of the United States of America, 116(36):17666–17672. **https://doi.org/10.1073/pnas.1907871116**

Klein, F., Marschall, H.R., Bowring, S.A., Humphris, S.E., and Horning, G., 2017. Mid-ocean ridge serpentinite in the Puerto Rico Trench: from seafloor spreading to subduction. Journal of Petrology, 58(9):1729–1754. **https://doi.org/10.1093/petrology/egx071**

Lambart, S., Koornneef, J.M., Millet, M.-A., Davies, G.R., Cook, M., and Lissenberg, C.J., 2019. Highly heterogeneous depleted mantle recorded in the lower oceanic crust. Nature Geoscience, 12(6):482–486. **https://doi.org/10.1038/s41561-019-0368-9**

Lang, S.Q., and Brazelton, W.J., 2020. Habitability of the marine serpentinite subsurface: a case study of the Lost City hydrothermal field. Philosophical Transactions of the Royal Society A: Mathematical, Physical and Engineering Sciences, 378(2165):20180429. **https://doi.org/10.1098/rsta.2018.0429**

Lang, S.Q., Butterfield, D.A., Schulte, M., Kelley, D.S., and Lilley, M.D., 2010. Elevated concentrations of formate, acetate and dissolved organic carbon found at the Lost City hydrothermal field. Geochimica et Cosmochimica Acta, 74(3):941–952. **https://doi.org/10.1016/j.gca.2009.10.045**

Lang, S.Q., Früh-Green, G.L., Bernasconi, S.M., Brazelton, W.J., Schrenk, M.O., and McGonigle, J.M., 2018. Deeply-sourced formate fuels sulfate reducers but not methanogens at Lost City hydrothermal field. Scientific Reports, 8(1):755. **https://doi.org/10.1038/s41598-017-19002-5**

Lang, S.Q., Früh-Green, G.L., Bernasconi, S.M., Lilley, M.D., Proskurowski, G., Méhay, S., and Butterfield, D.A., 2012. Microbial utilization of abiogenic carbon and hydrogen in a serpentinite-hosted system. Geochimica et Cosmochimica Acta, 92:82–99. **https://doi.org/10.1016/j.gca.2012.06.006**

Lang, S.Q., Lilley, M.D., Baumberger, T., Früh-Green, G.L., Walker, S.L., Brazelton, W.J., Kelley, D.S., Elend, M., Butterfield, D.A., and Mau, A.J., 2021. Extensive decentralized hydrogen export from the Atlantis Massif. Geology, 49(7):851–856. **https://doi.org/10.1130/G48322.1**

Lang, S.Q., McCaig, A.M, Blum, P., Abe, N., Brazelton, W., Coltat, R., Deans, J.R., Dickerson, K.L., Godard, M., John, B.E., Klein, F., Kuehn, R., Lin, K.-Y., Lissenberg, C.J., Liu, H., Lopes, E.L., Nozaka, T., Parsons, A.J., Pathak, V., Reagan, M.K., Robare, J.A., Savov, I.P., Schwarzenbach, E., Sissmann, O.J., Southam, G., Wang, F., and Wheat, C.G., 2025a. Expedition 399 methods. In McCaig, A.M., Lang, S.Q., Blum, P., and the Expedition 399 Scientists, Building

Blocks of Life, Atlantis Massif. Proceedings of the International Ocean Discovery Program, 399: College Station, TX (International Ocean Discovery Program). **https://doi.org/10.14379/iodp.proc.399.102.2025**

Lang, S.Q., McCaig, A.M, Blum, P., Abe, N., Brazelton, W., Coltat, R., Deans, J.R., Dickerson, K.L., Godard, M., John, B.E., Klein, F., Kuehn, R., Lin, K.-Y., Lissenberg, C.J., Liu, H., Lopes, E.L., Nozaka, T., Parsons, A.J., Pathak, V., Reagan, M.K., Robare, J.A., Savov, I.P., Schwarzenbach, E., Sissmann, O.J., Southam, G., Wang, F., and Wheat, C.G., 2025b. Site U1601. In McCaig, A.M., Lang, S.Q., Blum, P., and the Expedition 399 Scientists, Building Blocks of Life, Atlantis Massif. Proceedings of the International Ocean Discovery Program, 399: College Station, TX (International Ocean Discovery Program). **https://doi.org/10.14379/iodp.proc.399.104.2025**

Liebmann, J., Schwarzenbach, E.M., Früh-Green, G.L., Boschi, C., Rouméjon, S., Strauss, H., Wiechert, U., and John, T., 2018. Tracking water-rock interaction at the Atlantis Massif (MAR, 30°N) using sulfur geochemistry. Geochemistry, Geophysics, Geosystems, 19(11):4561–4583. **https://doi.org/10.1029/2018GC007813**

Lissenberg, C.J., and MacLeod, C.J., 2017. A reactive porous flow control on mid-ocean ridge magmatic evolution. Journal of Petrology, 57(11-12):2195–2220. **https://doi.org/10.1093/petrology/egw074**

Lissenberg, C.J., McCaig, A.M., Lang, S.Q., Blum, P., Abe, N., Brazelton, W.J., Coltat, R., Deans, J.R., Dickerson, K.L., Godard, M., John, B.E., Klein, F., Kuehn, R., Lin, K.-Y., Liu, H., Lopes, E.L., Nozaka, T., Parsons, A.J., Pathak, V., Reagan, M.K., Robare, J.A., Savov, I.P., Schwarzenbach, E.M., Sissmann, O.J., Southam, G., Wang, F., Wheat, C.G., Anderson, L., and Treadwell, S., 2024. A long section of serpentinized depleted mantle peridotite. Science, 385(6709):623–629. **https://doi.org/10.1126/science.adp1058**

Lowell, R.P., 2017. A fault-driven circulation model for the Lost City hydrothermal field. Geophysical Research Letters, 44(6):2703–2709. **https://doi.org/10.1002/2016GL072326**

Ludwig, K.A., Shen, C.-C., Kelley, D.S., Cheng, H., and Edwards, R.L., 2011. U–Th systematics and ^{230}Th ages of carbonate chimneys at the Lost City hydrothermal field. Geochimica et Cosmochimica Acta, 75(7):1869–1888. **https://doi.org/10.1016/j.gca.2011.01.008**

Magenheim, A.J., Spivack, A.J., Alt, J.C., Bayhurst, G., Chan, L.H., Zuleger, E., and Gieskes, J.M., 1995. Borehole fluid chemistry in Hole 504B, Leg 137: formation water or in-situ reaction. In Erzinger, J., Becker, K., Dick, H.J.B., and Stokking, L.B. (Eds.), Proceedings of the Ocean Drilling Program, Scientific Results. 137/140: College Station, TX (Ocean Drilling Program), 141–152. **https://doi.org/10.2973/odp.proc.sr.137140.024.1995**

Martin, W., Baross, J., Kelley, D., and Russell, M.J., 2008. Hydrothermal vents and the origin of life. Nature Reviews Microbiology, 6(11):805–814. **https://doi.org/10.1038/nrmicro1991**

Martin, W., and Russell, M.J., 2006. On the origin of biochemistry at an alkaline hydrothermal vent. Philosophical Transactions of the Royal Society B: Biological Sciences, 362:1887–1925. **https://doi.org/10.1098/rstb.2006.1881**

Mason, O.U., Nakagawa, T., Rosner, M., Van Nostrand, J.D., Zhou, J., Maruyama, A., Fisk, M.R., and Giovannoni, S.J., 2010. First investigation of the microbiology of the deepest layer of ocean crust. PLOS ONE, 5(11):e15399. **https://doi.org/10.1371/journal.pone.0015399**

McCaig, A., Lang, S.Q., and Blum, P., 2022. Expedition 399 Scientific Prospectus: Building Blocks of Life, Atlantis Massif. International Ocean Discovery Program. **https://doi.org/10.14379/iodp.sp.399.2022**

McCaig, A., Lang, S.Q., Blum, P., and the Expedition 399 Scientists, 2024. Expedition 399 Preliminary Report: Building Blocks of Life, Atlantis Massif. International Ocean Discovery Program. **https://doi.org/10.14379/iodp.pr.399.2024**

McCaig, A.M., Delacour, A., Fallick, A.E., Castelain, T., and Früh-Green, G.L., 2010. Detachment fault control on hydrothermal circulation systems: interpreting the subsurface beneath the TAG hydrothermal field using the isotopic and geological evolution of oceanic core complexes in the Atlantic. In Rona, P., Devey, C.W., Dyment, J., and Murton, B.J. (Eds.), Diversity of Hydrothermal Systems on Slow Spreading Ocean Ridges. Geophysical Monograph, 188: 207–239. **https://doi.org/10.1029/2008GM000729**

McCaig, A.M., and Harris, M., 2012. Hydrothermal circulation and the dike-gabbro transition in the detachment mode of slow seafloor spreading. Geology, 40(4):367–370. **https://doi.org/10.1130/G32789.1**

McCaig, A.M, Lang, S.Q., Blum, P., Abe, N., Brazelton, W., Coltat, R., Deans, J.R., Dickerson, K.L., Godard, M., John, B.E., Klein, F., Kuehn, R., Lin, K.-Y., Lissenberg, C.J., Liu, H., Lopes, E.L., Nozaka, T., Parsons, A.J., Pathak, V., Reagan, M.K., Robare, J.A., Savov, I.P., Schwarzenbach, E., Sissmann, O.J., Southam, G., Wang, F., and Wheat, C.G., 2025. Site U1309. In McCaig, A.M., Lang, S.Q., Blum, P., and the Expedition 399 Scientists, Building Blocks of Life, Atlantis Massif. Proceedings of the International Ocean Discovery Program, 399: College Station, TX (International Ocean Discovery Program). **https://doi.org/10.14379/iodp.proc.399.103.2025**

McCollom, T.M., and Bach, W., 2009. Thermodynamic constraints on hydrogen generation during serpentinization of ultramafic rocks. Geochimica et Cosmochimica Acta, 73(3):856–875. **https://doi.org/10.1016/j.gca.2008.10.032**

McCollom, T.M., Klein, F., Robbins, M., Moskowitz, B., Berquó, T.S., Jöns, N., Bach, W., and Templeton, A., 2016. Temperature trends for reaction rates, hydrogen generation, and partitioning of iron during experimental serpentinization of olivine. Geochimica et Cosmochimica Acta, 181:175–200. **https://doi.org/10.1016/j.gca.2016.03.002**

McCollom, T.M., and Seewald, J.S., 2007. Abiotic synthesis of organic compounds in deep-sea hydrothermal environments. Chemical Reviews, 107(2):382–401. **https://doi.org/10.1021/cr0503660**

McCollom, T.M., and Seewald, J.S., 2013. Serpentinites, hydrogen, and life. Elements, 9(2):129–134. **https://doi.org/10.2113/gselements.9.2.129**

McDermott, J.M., Seewald, J.S., German, C.R., and Sylva, S.P., 2015. Pathways for abiotic organic synthesis at submarine hydrothermal fields. Proceedings of the National Academy of Sciences of the United States of America, 112(25):7668–7672. **https://doi.org/10.1073/pnas.1506295112**

McGonigle, J.M., Lang, S.Q., Brazelton, W.J., and Parales, R.E., 2020. Genomic evidence for formate Metabolism by Chloroflexi as the key to unlocking deep carbon in Lost City microbial ecosystems. Applied and Environmental Microbiology, 86(8):e02583-02519. **https://doi.org/10.1128/AEM.02583-19**

Méhay, S., Früh-Green, G.L., Lang, S.Q., Bernasconi, S.M., Brazelton, W.J., Schrenk, M.O., Schaeffer, P., and Adam, P., 2013. Record of archaeal activity at the serpentinite-hosted Lost City hydrothermal field. Geobiology, 11(6):570–592. **https://doi.org/10.1111/gbi.12062**

Ménez, B., Pisapia, C., Andreani, M., Jamme, F., Vanbellingen, Q.P., Brunelle, A., Richard, L., Dumas, P., and Réfrégiers, M., 2018. Abiotic synthesis of amino acids in the recesses of the oceanic lithosphere. Nature, 564(7734):59–63. **https://doi.org/10.1038/s41586-018-0684-z**

Michibayashi, K., Hirose, T., Nozaka, T., Harigane, Y., Escartin, J., Delius, H., Linek, M., and Ohara, Y., 2008. Hydration due to high-T brittle failure within in situ oceanic crust, 30°N Mid-Atlantic Ridge. Earth and Planetary Science Letters, 275(3–4):348–354. **https://doi.org/10.1016/j.epsl.2008.08.033**

Morris, A., Gee, J.S., Pressling, N., John, B.E., MacLeod, C.J., Grimes, C.B., and Searle, R.C., 2009. Footwall rotation in an oceanic core complex quantified using reoriented Integrated Ocean Drilling Program core samples. Earth and Planetary Science Letters, 287(1–2):217–228. **https://doi.org/10.1016/j.epsl.2009.08.007**

Motamedi, S., Orcutt, B.N., Früh-Green, G.L., Twing, K.I., Pendleton, H.L., and Brazelton, W.J., 2020. Microbial residents of the Atlantis Massif's shallow serpentinite subsurface. Applied and Environmental Microbiology, 86(11):e00356-00320. **https://doi.org/10.1128/AEM.00356-20**

Natland, J.H., and Dick, H.J.B., 2002. Stratigraphy and composition of gabbros drilled in Ocean Drilling Program Hole 735B, Southwest Indian Ridge: a synthesis of geochemical data. In Natland, J.H., Dick, H.J.B., Miller, D.J., and Von Herzen, R.P. (Eds.), Proceedings of the Ocean Drilling Program, Scientific Results. 176: College Station, TX (Ocean Drilling Program). **https://doi.org/10.2973/odp.proc.sr.176.002.2002**

Nozaka, T., and Fryer, P., 2011. Alteration of the oceanic lower crust at a slow-spreading axis: insight from vein-related zoned halos in olivine gabbro from Atlantis Massif, Mid-Atlantic Ridge. Journal of Petrology, 52(4):643–664. **https://doi.org/10.1093/petrology/egq098**

Nozaka, T., Fryer, P., and Andreani, M., 2008. Formation of clay minerals and exhumation of lower-crustal rocks at Atlantis Massif, Mid-Atlantic Ridge. Geochemistry, Geophysics, Geosystems, 9(11):Q11005. **https://doi.org/10.1029/2008GC002207**

Pendleton, H.L., Twing, K.I., Motamedi, S., and Brazelton, W.J., 2021. Potential microbial contamination from drilling lubricants into subseafloor rock cores. Scientific Drilling, 29:49–57. **https://doi.org/10.5194/sd-29-49-2021**

Pisapia, C., Jamme, F., Duponchel, L., and Ménez, B., 2018. Tracking hidden organic carbon in rocks using chemometrics and hyperspectral imaging. Scientific Reports, 8(1):2396. **https://doi.org/10.1038/s41598-018-20890-4**

Pressling, N., Morris, A., John, B.E., and MacLeod, C.J., 2012. The internal structure of an oceanic core complex: an integrated analysis of oriented borehole imagery from IODP Hole U1309D (Atlantis Massif). Geochemistry, Geophysics, Geosystems, 13(9):Q04G01. **https://doi.org/10.1029/2012GC004061**

Proskurowski, G., Lilley, M.D., Seewald, J.S., Früh-Green, G.L., Olson, E.J., Lupton, J.E., Sylva, S.P., and Kelley, D.S., 2008. Abiogenic hydrocarbon production at Lost City hydrothermal field. Science, 319(5863):604–607. **https://doi.org/10.1126/science.1151194**

Quéméneur, M., Erauso, G., Frouin, E., Zeghal, E., Vandecasteele, C., Ollivier, B., Tamburini, C., Garel, M., Ménez, B., and Postec, A., 2019. Hydrostatic pressure helps to cultivate an original anaerobic bacterium from the Atlantis Massif subseafloor (IODP Expedition 357): Petrocella atlantisensis gen. nov. sp. nov. Frontiers in Microbiology, 10:1497. **https://doi.org/10.3389/fmicb.2019.01497**

Rouméjon, S., Früh-Green, G.L., Orcutt, B.N., and the IODP Expedition 357 Science Party, 2018a. Alteration heterogeneities in peridotites exhumed on the southern wall of the Atlantis Massif (IODP Expedition 357). Journal of Petrology, 59(7):1329–1358. **https://doi.org/10.1093/petrology/egy065**

Rouméjon, S., Williams, M.J., and Früh-Green, G.L., 2018b. In-situ oxygen isotope analyses in serpentine minerals: constraints on serpentinization during tectonic exhumation at slow- and ultraslow-spreading ridges. Lithos, 323:156–173. **https://doi.org/10.1016/j.lithos.2018.09.021**

Sawyer, D.S., Whitmarsh, R.B., Klaus, A., et al., 1994. Proceedings of the Ocean Drilling Program, Initial Reports, 149: College Station, TX (Ocean Drilling Program). **https://doi.org/10.2973/odp.proc.ir.149.1994**

Schoolmeesters, N., Cheadle, M.J., John, B.E., Reiners, P.W., Gee, J., and Grimes, C.B., 2012. The cooling history and the depth of detachment faulting at the Atlantis Massif oceanic core complex. Geochemistry, Geophysics, Geosystems, 13(10):Q0AG12. **https://doi.org/10.1029/2012GC004314**

Schrenk, M.O., Brazelton, W.J., and Lang, S.Q., 2013. Serpentinization, carbon, and deep life. Reviews in Mineralogy and Geochemistry, 75(1):575–606. **https://doi.org/10.2138/rmg.2013.75.18**

Schrenk, M.O., Kelley, D.S., Bolton, S.A., and Baross, J.A., 2004. Low archaeal diversity linked to subseafloor geochemical processes at the Lost City hydrothermal field, Mid-Atlantic Ridge. Environmental Microbiology, 6(10):1086–1095. **https://doi.org/10.1111/j.1462-2920.2004.00650.x**

Schroeder, T., and John, B.E., 2004. Strain localization on an oceanic detachment fault system, Atlantis Massif, 30°N, Mid-Atlantic Ridge. Geochemistry, Geophysics, Geosystems, 5(11):Q11007. **https://doi.org/10.1029/2004GC000728**

Seyfried, W.E., Pester, N.J., Tutolo, B.M., and Ding, K., 2015. The Lost City hydrothermal system: constraints imposed by vent fluid chemistry and reaction path models on subseafloor heat and mass transfer processes. Geochimica et Cosmochimica Acta, 163:59–79. **https://doi.org/10.1016/j.gca.2015.04.040**

Sojo, V., Herschy, B., Whicher, A., Camprubí, E., and Lane, N., 2016. The origin of life in alkaline hydrothermal vents. Astrobiology, 16(2):181–197. **https://doi.org/10.1089/ast.2015.1406**

Stüeken, E.E., Anderson, R.E., Bowman, J.S., Brazelton, W.J., Colangelo-Lillis, J., Goldman, A.D., Som, S.M., and Baross, J.A., 2013. Did life originate from a global chemical reactor? Geobiology, 11(2):101–126. **https://doi.org/10.1111/gbi.12025**

Suhr, G., Hellebrand, E., Johnson, K., and Brunelli, D., 2008. Stacked gabbro units and intervening mantle; a detailed look at a section of IODP Leg 305, Hole U1309D. Geochemistry, Geophysics, Geosystems, 9(10):Q10007. **https://doi.org/10.1029/2008GC002012**

Summit, M., and Baross, J.A., 2001. A novel microbial habitat in the mid-ocean ridge subseafloor. Proceedings of the National Academy of Sciences of the United States of America, 98(5):2158–2163. **https://doi.org/10.1073/pnas.051516098**

Sylvan, J.B., Estes, E.R., Bogus, K., Colwell, F.S., Orcutt, B.N., and Smith, D.C, 2021. Technical Note 4: Recommendations for microbiological sampling and contamination tracer use aboard the JOIDES Resolution following 20 years of IODP deep biosphere research. International Ocean Discovery Program Technical Note. **https://doi.org/10.14379/iodp.tn.4.2021**

Tamura, A., Arai, S., Ishimaru, S., and Andal, E.S., 2008. Petrology and geochemistry of peridotites from IODP Site U1309 at Atlantis Massif, MAR 30°N: micro- and macro-scale melt penetrations into peridotites. Contributions to Mineralogy and Petrology, 155(4):491–509. **https://doi.org/10.1007/s00410-007-0254-0**

Teagle, D.A.H., Alt, J.C., Umino, S., Miyashita, S., Banerjee, N.R., Wilson, D.S., and the Expedition 309/312 Scientists, 2006. Proceedings of the Integrated Ocean Drilling Program, 309/312: Washington, DC (Integrated Ocean Drilling Program Management International, Inc.). **https://doi.org/10.2204/iodp.proc.309312.2006**

Ternieten, L., Früh-Green, G.L., and Bernasconi, S.M., 2021. Distribution and sources of carbon in serpentinized mantle peridotites at the Atlantis Massif (IODP Expedition 357). Journal of Geophysical Research: Solid Earth, 126(10):e2021JB021973. **https://doi.org/10.1029/2021JB021973**

Titarenko, S.S., and McCaig, A.M., 2016. Modelling the Lost City hydrothermal field: influence of topography and permeability structure. Geofluids, 16(2):314–328. **https://doi.org/10.1111/gfl.12151**

Wang, D.T., Reeves, E.P., McDermott, J.M., Seewald, J.S., and Ono, S., 2018. Clumped isotopologue constraints on the origin of methane at seafloor hot springs. Geochimica et Cosmochimica Acta, 223:141–158. **https://doi.org/10.1016/j.gca.2017.11.030**

Whitmarsh, R.B., Beslier, M.-O., Wallace, P.J., Abe, N., Basile, C., Beard, J.S., Froitzheim, N., Gardien, V., Hébert, R., Hopkinson, L.J., Kudless, K.E., Louvel, V., Manatschal, G., Newton, A.C., Rubenach, M.J., Skelton, A.D.L., Smith, S.E., Takayama, H., Tompkins, M.J., Turrin, B.D., Urquhart, E., Wallrabe-Adams, H.-J., Wilkens, R.H., Wilson, R.C.L., Wise, S.W., Jr., and Zhao, X., 1998. Proceedings of the Ocean Drilling Program, Initial reports, 173: College Station, TX (Ocean Drilling Program). **http://doi.org/10.2973/odp.proc.ir.173.1998**